Supplementary Appendix

This appendix has been provided by the authors to give readers additional information about their work.

Supplement to: Kajstura J, Rota M, Hall SR, et al. Evidence for human lung stem cells. N Engl J Med 2011;364:1795-806.

Legends to Supplementary Figures

Figure 1. Culture of hLSCs. In vitro expansion of sorted c-kit-positive cells over time (green).

Figure 2. hLSC Phenotype. Panel A: Bivariate distribution plots of CD34-positive human bone marrow cells after collagenase treatment, and human lung cells negative for c-kit. SSC: side scatter. Panel B: Bivariate distribution plots of c-kit-positive cells negative for hematopoietic cell lineages (CD34, CD45, CD133, cocktail of bone marrow lineage markers), mesenchymal stromal cell antigens (CD44, CD90, CD105), and mast cell epitopes (CD45, tryptase, CD6, CD29, CD49d, CD49e). Panel C: The c-kit-positive cells are largely negative for markers of lung cells (TTF1, p63, CK5, pan-CK, SPC, Ets1, GATA6, vWf, α-SMA). Panel D: hLSC clones in Terasaki plates. Clones generated by c-kit positive lineage-negative cells continue to express the stem cell marker. Cloning efficiency is shown in individual cases and as mean ± SD. Panel E: Bivariate distribution plots of c-kit and epitopes specific for lung cell classes document the undifferentiated phenotype of clonal hLSCs.

Figure 3. Expression of c-kit and Lineage Markers in hLSCs. Panel A: qRT-PCR and immunoprecipitation/Western blotting of clonal hLSCs, hCSCs, and bone marrow cells (BM). C-kit protein was detected at 145 and 120 kDa. The mature form of the receptor capable of binding to stem cell factor has a molecular weight of 145 kDa. Panel B: Nucleotide sequences obtained in sense and anti-sense directions confirmed that the amplified PCR products corresponded to the expected c-kit human gene. Panel C: qRT-PCR of transcripts for TTF1, p63, CK5, SPC, CC10, and CFTR. Representative curves

and PCR products are shown. Human β2microglobulin (B2M) was used as housekeeping gene.

Figure 4. Differentiation of hLSCs. Panel A: Bivariate distribution plots of clonal lineage negative c-kit-positive hLSCs following exposure to dexamethasone; hLSCs expressed markers of epithelial cells (TTF1, p63, pan-CK, CK5, SPC), ECs (Ets1, vWf), and SMCs (GATA6, α-SMA). Panel B: Differentiating clonal c-kit-positive cells express TTF1 (white), SPC (magenta), pan-CK (red), Ets1 (yellow), vWf (bright blue), GATA6 (white), and α-SMA (yellow). Panel C: Quantitative data collected by FACS and immunolabeling. Values are shown as mean ± SD. Panel D: hLSCs do not acquire the myocyte lineage, and hCSCs do not form lung epithelial cells.

Figure 5. hLSCs and Pluripotency Genes. Panel A: Immunolabeling of NANOG (white), OCT3/4 (yellow), SOX2 (magenta), and KLF4 (bright blue) in undifferentiated clonal c-kit-positive hLSCs (green). Panel B: Nucleotide sequences obtained in sense and anti-sense directions confirmed that the amplified PCR products corresponded to the expected human genes.

Figure 6. Division of Clonal hLSC. Panel A: Dividing hLSC in which chromosomes are organized in telophase (left panel); α-adaptin is uniformly distributed in the dividing stem cell (central panel, blue), documenting symmetric division. Right panel, merge. Panel B: Dividing hLSC in which chromosomes are organized in telophase (left panel); α-adaptin is not uniformly distributed in the dividing stem cell (central panel, blue), demonstrating asymmetric division. The absence of TTF1 in one of the daughter cells and the presence of TTF1 (arrow) in the other suggests the formation of a daughter stem cell and an early committed epithelial cell. Panel C: Dividing hLSC in which chromosomes are organized

in telophase (left panel); α-adaptin is not uniformly distributed in the dividing stem cell (central panel, blue), documenting asymmetric division. The absence of Ets1 in one of the daughter cells and the presence of Ets1 in the other (arrow) suggests the formation of a daughter stem cell and an early committed EC.

Figure 7. Cryoinjured Lesion of the Lung. Panel A: Mouse lung one day following cryoinjury. Illustration of a single injection of clonal c-kit-EGFP-positive hLSCs mixed with 1% rhodamine-labeled microspheres (RM) delivered in proximity to the cryoinjured region of the lung (CI). Panel B: Shortly after cryoinjury, epithelial cells are positive for TdT labeling of nuclei (white) and show residual labeling for pan-CK (red). Panel C: At 14 days after cryoinjury, fibroblasts (procoll, magenta) replace the damaged parenchyma. A few apoptotic nuclei, positive for TdT (white), are also present.

Figure 8. Division of Clonal hLSCs In Vivo. Panels A-C: Symmetric (arrows) and asymmetric (arrowheads) division of clonal EGFP-positive hLSCs (green) 2 days after injection in proximity to the injured lung; α-adaptin (magenta) is uniformly distributed in the dividing cells (arrows) or is restricted to one of the two daughter cells (arrowheads). TTF1, GATA6, or Ets1 is expressed in the committed hLSCs (asterisks). Nuclei, DAPI (white). Panel D: Data are shown as mean ± SD. C, clonal: NC, non-clonal.

Figure 9. hLSCs and Lung Regeneration. Ten days after non-clonal-hLSC delivery, the cryoinjured (CI) region is partially replaced by EGFP-positive (upper left, green), Alu-positive (upper central, white), and pan-CK-positive (upper right, red) human alveoli, which are shown at higher magnification in the insets. Recipient mouse epithelial cells, positive for pan-CK but EGFP-negative, are present at the periphery of the regenerated tissue. The yellow dotted line defines this boundary. The regenerated lung contains

EGFP-positive vascular profiles (lower panels); they are included in the small rectangles at low magnification and are then shown at higher magnification in the insets. ECs are positive for EGFP (left, green), Alu (central: white, arrowheads), and vWf (right, magenta).

Figure 10. hLSCs Generate Alveoli In Vivo. Clonal (upper panel) and non-clonal (lower panel) hLSCs formed alveoli expressing EGFP (green) and pro-SPC (red) or SPC (red).

Figure 11. hLSCs Generate Bronchioles In Vivo. Panel A: EGFP-positive (upper left) pan-CK-positive (upper right) human bronchiole. A thin layer of SMCs, positive for α-SMA (bright blue), is also present (upper right). Alu sequences (lower left, white dots). Lower right, merge. Panel B: Cluster of EGFP-positive hLSCs (upper left) in the initial stages of epithelial cell organization (open arrows), adjacent to a recipient mouse bronchiole (asterisks), which is EGFP-negative (upper left). Both structures are pan-CK-positive (upper right) and α-SMA-negative (lower left). Lower right, merge. Panel C: EGFP-positive hLSCs (upper left) in the initial stages of epithelial cell organization (open arrows) and a newly-formed, well-developed EGFP-positive human bronchiole (arrows) are adjacent to a recipient EGFP-negative mouse bronchiole (asterisks). These structures are pan-CK-positive (upper right) and α-SMA-negative (lower left). A recipient mouse vessel (v), which is EGFP-negative and α-SMA-positive, is present in the same field. Lower right, merge. Inset, Note the cytoplasmic localization of α-SMA and pan-CK. Panel D: Newly-formed, EGFP-positive human bronchiole (arrows) is adjacent to a recipient EGFP-negative (upper left) mouse bronchiole (asterisks). Both structures are pan-CK-positive (upper right) and α-SMA-negative (lower left). Lower right, merge.

Figure 12. hLSCs Generate Pulmonary Vessels. Panel A: Examples of newly-formed human pulmonary arterioles. In all cases, the vessel wall is composed of EGFP-positive (left, green) SMCs, expressing α-SMA (central, red), and ECs, expressing vWf (central, bright blue). Right, merge. In the lower right panel the localization of Alu is shown (white dots).

Figure 13. Lung Regeneration. Lung regeneration by clonal (C) and non-clonal (NC) hLSCs.

Figure 14. Spectral Analysis. Panels A-J: Emission spectra from native EGFP (A), and immunolabeled EGFP (B), pan-CK (C), pro-SPC (D), SPC (E), CC10 (F), AP-5 (G), Alu (H), α-SMA (I), and vWf (J). The signals from EGFP and all other labels are represented by green lines, while tissue autofluorescence is illustrated by the blue lines. Note the difference in the intensity of the signals at wavelengths reflecting maximum fluorescence in each case. Following normalization for the intensity of the signals for each label, all emission spectra were essentially superimposable. In contrast, the emission spectra for tissue autofluorescence had a different shape and were easily distinguishable from the specific signals of native EGFP and immunolabeled proteins.

Figure 15. Human HSCs and hCSCs. Panel A: Four EGFP-positive (green, arrows) undifferentiated hCSCs are seen 10 days after cryoinjury and cell implantation. Panel B: Three Alu-positive human HSCs (white nuclear dots, arrows) are seen in the damaged lung.

Figure 16. Expression of Human Genes and Lung Regeneration. Panel A: Transcripts of human epithelial cell genes (TTF1, TP63, CFTR, Krt18, CC10, SFTPC, AQP5, T1α), EC genes (ETS1, PECAM1), and SMC gene (TGFBR1). β2-microglobulin (B2M) and β-

actin (ACTB) were used as housekeeping genes. ACTB primers identify β-actin in both mouse and human lungs. Additionally, mouse and human lung were used as negative and positive controls, respectively. Panel B: Nucleotide sequences obtained in sense and anti-sense directions confirmed that the amplified PCR products corresponded to the expected human genes.

Figure 17. Absence of Evidence for Cell Fusion. Panels A-E: Bronchiolar epithelial cells are EGFP-positive (A) and pan-CK-positive (B). In the lower region of this field, alveoli are EGFP-negative and correspond to the recipient mouse lung. Panel C: merge. The two areas included in the rectangles (C) are shown at higher magnification (D and E). Regenerated, EGFP-positive, pan-CK-positive bronchiolar epithelial cells carry only human X-chromosomes (D: hX-Chr, white dots). Alveolar epithelial cells from the recipient mouse lung are EGFP-negative and carry only mouse X-chromosomes (E: mX-Chr, magenta dots).

Figure 18. Absence of Evidence for Cell Fusion. Panels A-C: The epithelial cells of newly formed alveoli are EGFP-positive (A) and pan-CK-positive (B). Panel C: merge. The area included in the rectangle is shown at higher magnification in the lower panels. EGFP-positive pan-CK-positive alveolar epithelial cells carry only human X-chromosomes (hX-Chr, white dots).

Figure 19. Absence of Evidence for Cell Fusion. Panels A-C: Regenerated vessel composed of EGFP-positive (A) ECs (B: vWf, bright blue) and SMCs (B: α-SMA, red). Panel C: merge. The area included in the rectangle is shown at higher magnification in the lower panels. EGFP-positive vWf-positive and EGFP-positive α-SMA-positive vascular cells carry only human X-chromosomes (hX-Chr, white dots). Mouse X-

chromosomes (mX-Chr, magenta dots) are located outside the wall of the regenerated vessel.

Figure 20. Scheme of Ex Vivo Experiments by Two-Photon Microscopy. As shown in the left part of the scheme, airways were perfused continuously with an oxygenated Tyrode solution containing rhodamine-labeled dextran, which has a MW of 70,000 Da and red fluorescence. Pre-existing mouse alveoli and regenerated human alveoli were identified by the absence and presence of EGFP labeling, respectively. In this preparation, structures positive for EGFP but negative for rhodamine reflected newly formed vessels. In a complementary protocol shown in the right part of the scheme, the pulmonary artery was perfused in an identical manner and pre-existing mouse vessels and regenerated human vessels were identified by the absence and presence of EGFP labeling of the vessel wall, respectively. In this preparation, structures positive for EGFP but negative for rhodamine reflected newly formed alveoli. Two examples are provided in the lower two panels to illustrate the appearance of alveoli (left) and distal pulmonary vessels (right) in a normal intact mouse lung.

Figure 21. Integration of Regenerated Lung Structures. Panels A and B: Airways were perfused with rhodamine-labeled dextran. The red structures (A, left) correspond to individual alveoli (a) which are EGFP-positive (A, central). Right, merge. Structures positive for EGFP (A, central) but negative for rhodamine (A, left) reflect newly formed vessels (v). The area in the rectangle (A) is shown at higher magnification (B). Two alveoli and several vessels are in close proximity. Panels C and D: The pulmonary vasculature was perfused with rhodamine-labeled dextran. The red structures (C, left) correspond to distal pulmonary vessels (v) which are EGFP-positive (C, central). Right,

merge. Structures positive for EGFP (C, central) but negative for rhodamine (C, left) correspond to newly formed alveoli (a). The areas in rectangles (C) are shown at higher magnification (D). Two vessels and several alveoli are in close proximity.

Figure 22. Localization of hLSCs in Bronchioles. Panel A: Bronchiole, ~1.2 mm in diameter, with epithelial cells, positive for pan-CK, and SMCs, positive for α-SMA. Cartilage is also seen (bright blue). The basal cells of the epithelial lining express p63 in their nuclei (white). Several c-kit-positive cells (green) are present within the bronchiolar wall and its proximity. The 4 areas included in the rectangles are shown sequentially at higher magnification in the subsequent panels. In all cases, the basal epithelium also contains c-kit-positive cells which express p63 in their nuclei (white) and cytokeratin 5 (CK5, magenta; arrows) in their cytoplasm (see insets). The basal epithelium contains also c-kit-positive cells negative for p63 and CK5 (asterisks). Panel B: Bronchiole composed of pan-CK-positive epithelial cells (red). C-kit-positive cells are present within the bronchiolar wall and its proximity. The 3 areas included in the rectangles are shown sequentially at higher magnification in the lower panels. C-kit-positive cells (green) are connected by E-cadh (white, arrows) to bronchiolar epithelial cells (Area 1), SMCs (α-SMA, yellow; Area 2), and fibroblasts (procoll, bright blue; Area 3).

Figure 23. hLSCs and Fetal Lung. Three examples of fetal lungs with scattered c-kit-positive cells (green, arrows), negative for a combination of transcription factors (TFs) typical of lung cells ascertained simultaneously (TFs: TTF1, p63, Ets1, GATA6; yellow). Insets: c-kit-positive cells are connected by E-cadh (white; arrowheads) to epithelial cells of non-expanded alveoli.

Figure 24. hLSCs and Committed Cells. Panel A: An epithelial progenitor located in the alveolar wall (pan-CK, red) is shown at higher magnification in the inset; this progenitor cell retains the stem cell antigen c-kit (green) and expresses the epithelial transcription factor TTF1 (white, arrow). Panel B: An epithelial precursor within the alveolar wall is shown at higher magnification in the inset. This cell is positive for c-kit and pro-SPC (white, arrow). Panel C: Another epithelial precursor positive for c-kit and pan-CK (arrow) is apparent in the bronchiolar epithelium. Panel D: Endothelial and SMC progenitors located in the arteriolar wall are illustrated at higher magnification in the insets. These progenitor cells are c-kit-positive and express Ets1 (magenta) or GATA6 (white). von Willebrand factor (vWf), bright blue; α-smooth muscle actin (α-SMA), yellow.

Figure 25. Quantitative Analysis of hLSCs in the Adult Lung. Panel A: Number and distribution of adult hLSCs. Results are shown as means ± SD. *$P<0.05$ vs. bronchioles (Bro). Alv, alveoli; Epith, epithelial cells; CT, connective tissue. Panel B: Distribution of hLSCs in alveoli and bronchioles of different size.

Figure 26. Embryonic-Fetal Lung. Panel A: Embryonic-fetal lungs with scattered c-kit-positive cells (green, arrows), positive for NANOG (white), OCT3/4 (yellow), SOX2 (magenta), and KLF4 (bright blue). Collapsed lung tissue is labeled by pan-CK (red). Panels B: c-kit-positive cells (green, arrows) express TTF1 (white), p63 (yellow), Ets1 (magenta), and GATA6 (bright blue). Collapsed lung tissue is labeled by pan-CK (red). Panel C: Number of embryonic-fetal hLSCs in the 9 samples examined. Gestational age is indicated in weeks.

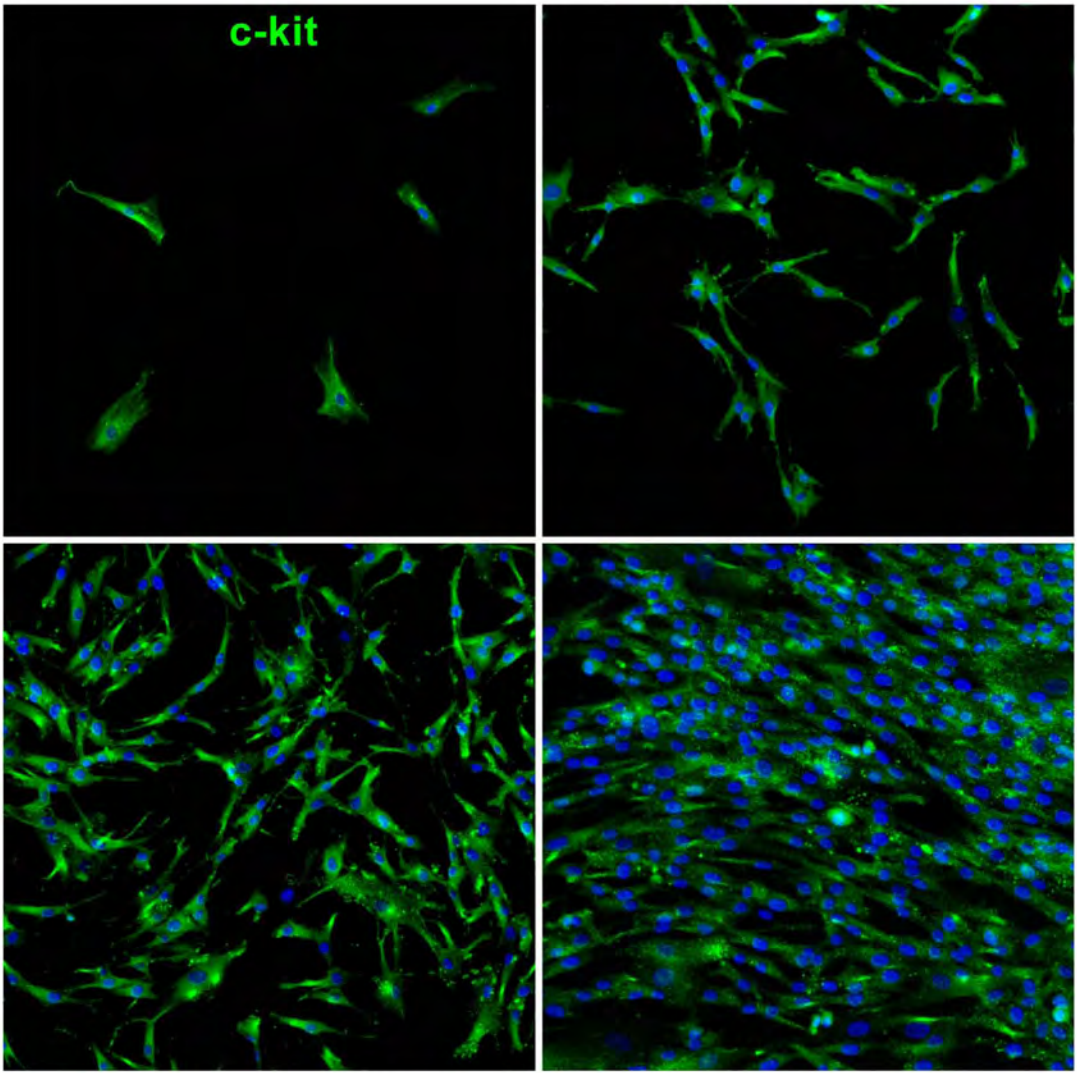

Supplementary Figure 1

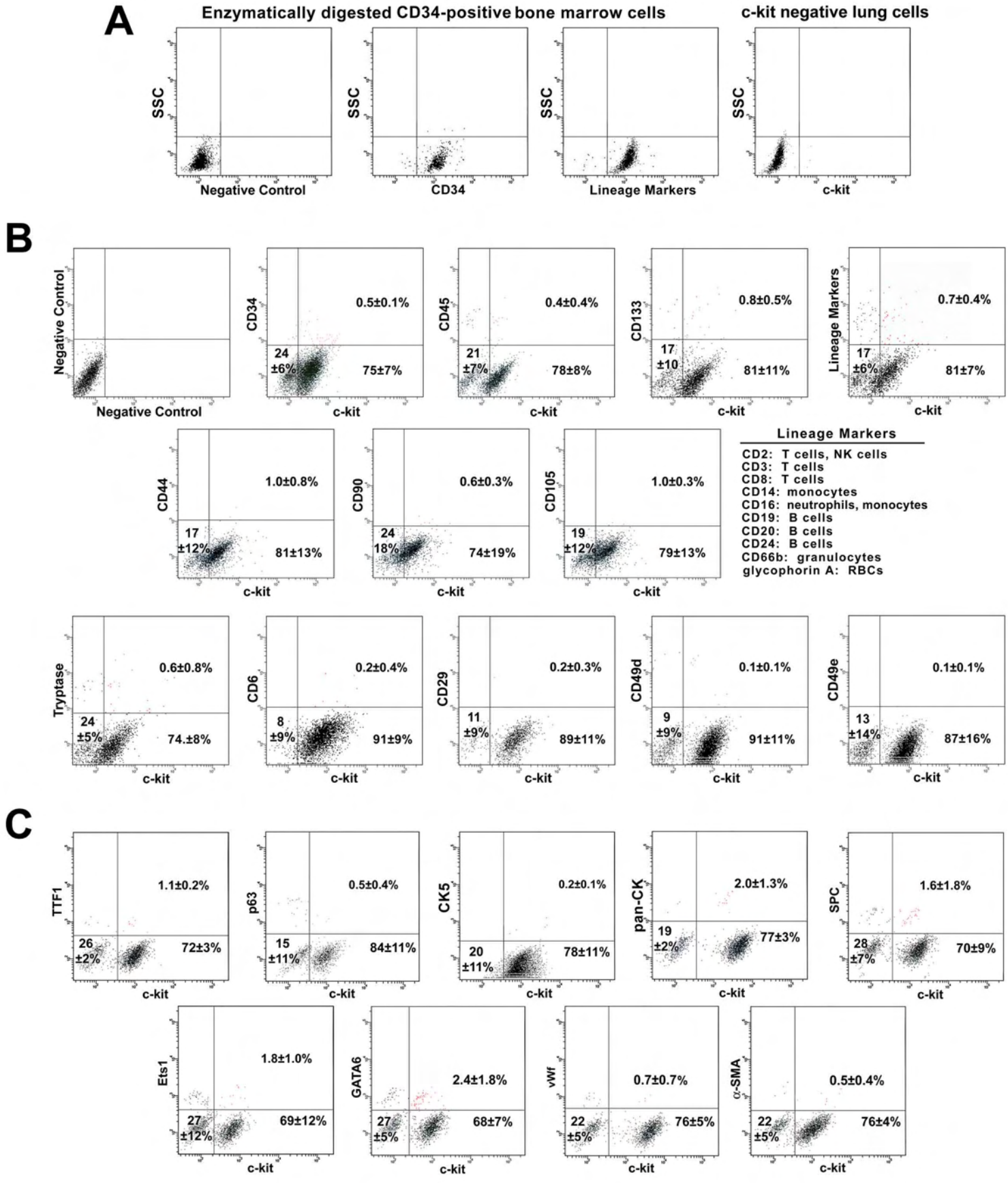

Supplementary Figure 2A-C

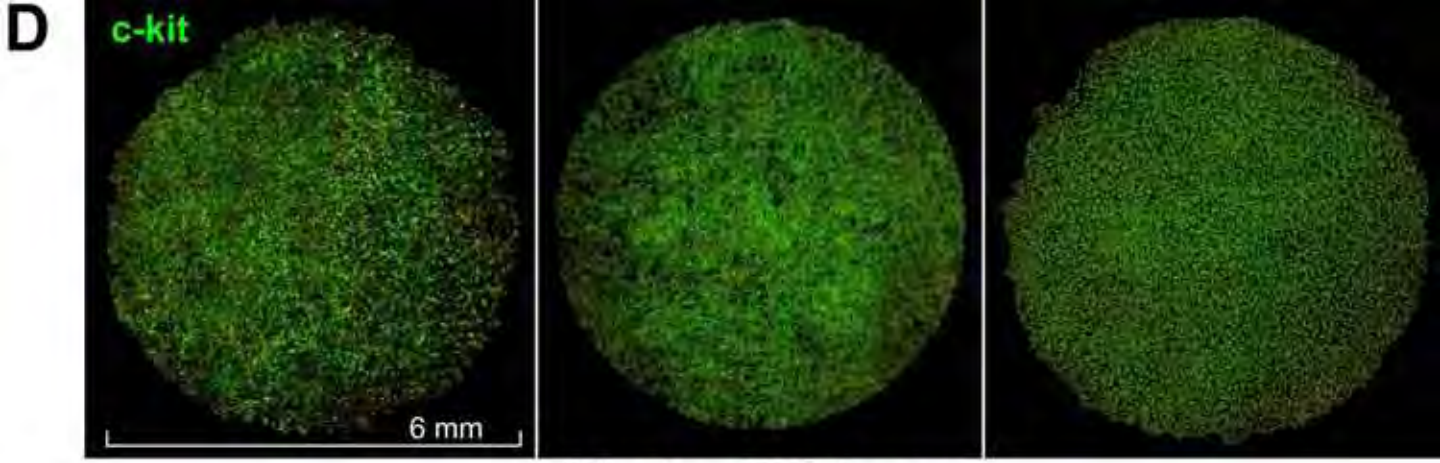

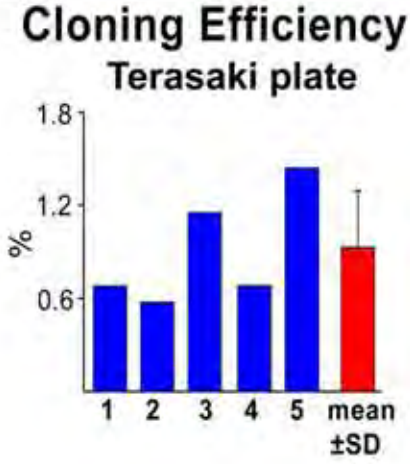

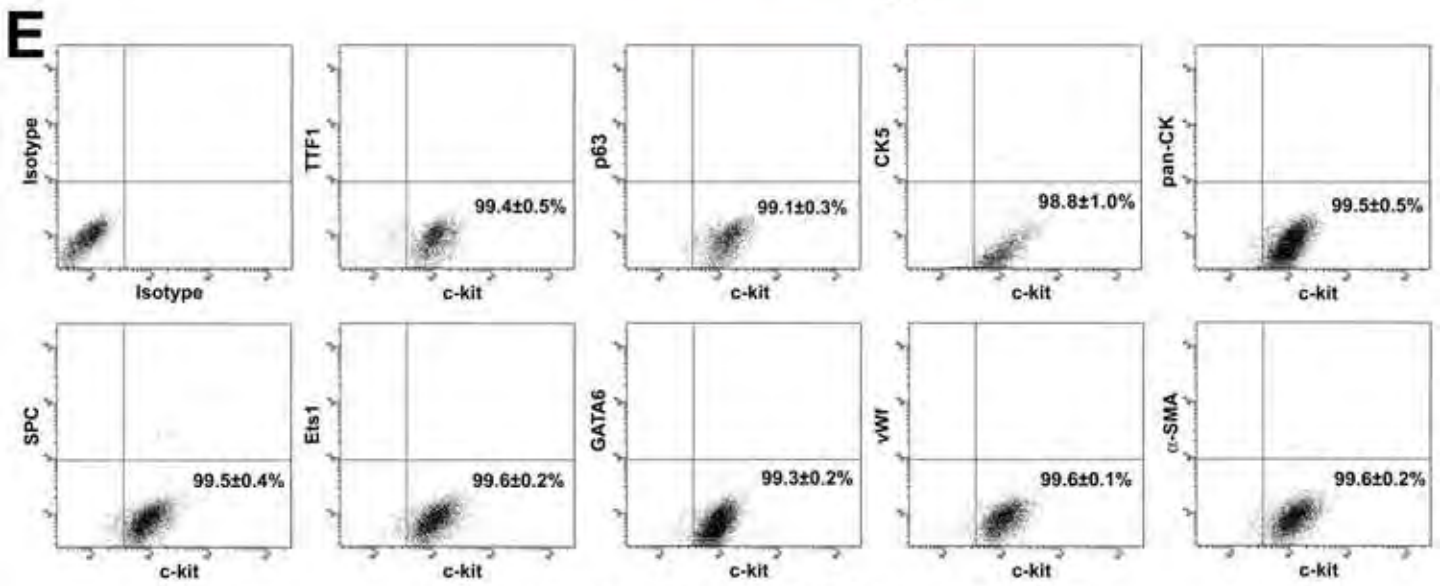

Supplementary Figure 2D, E

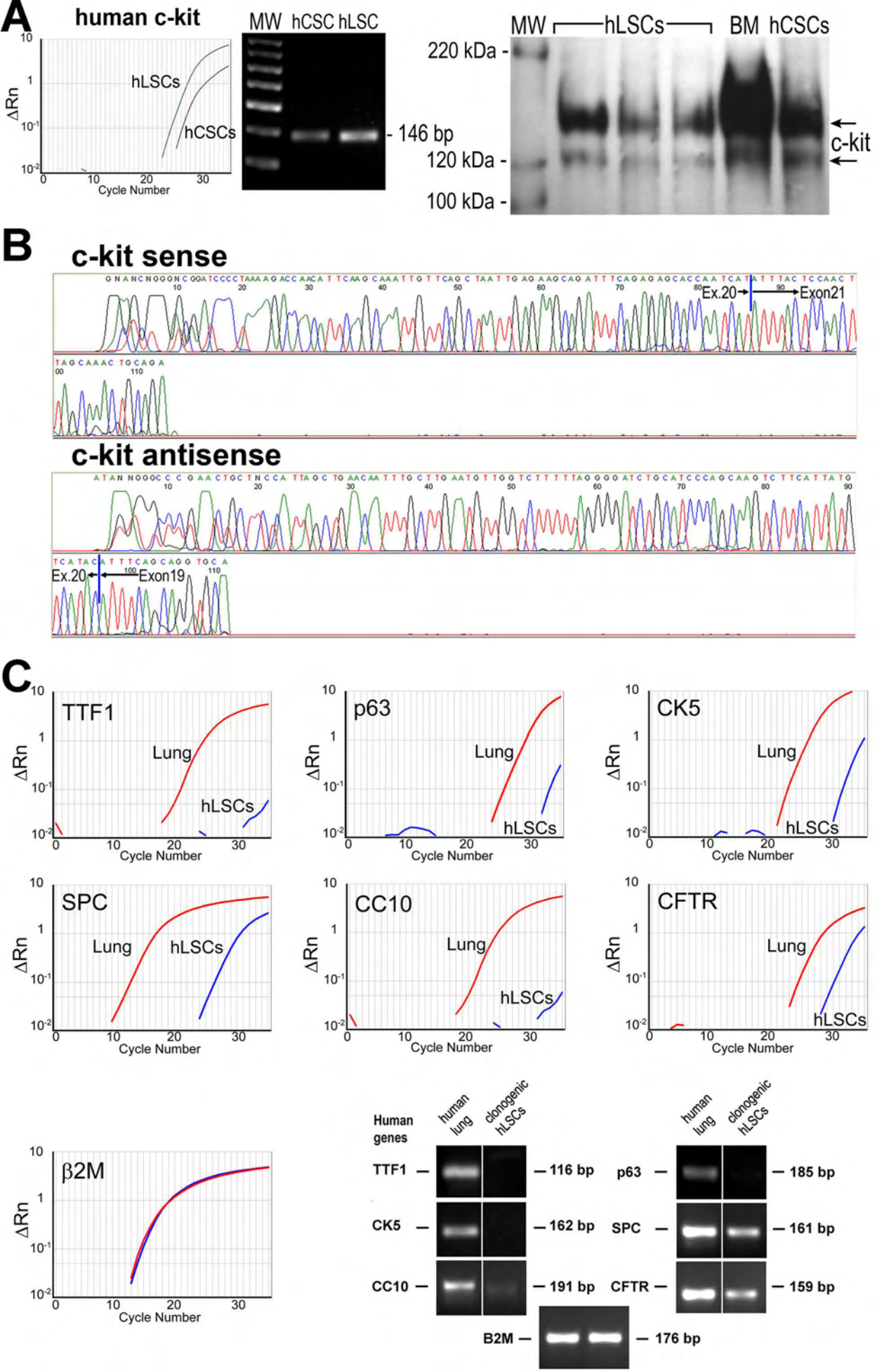

Supplementary Figure 3A-C

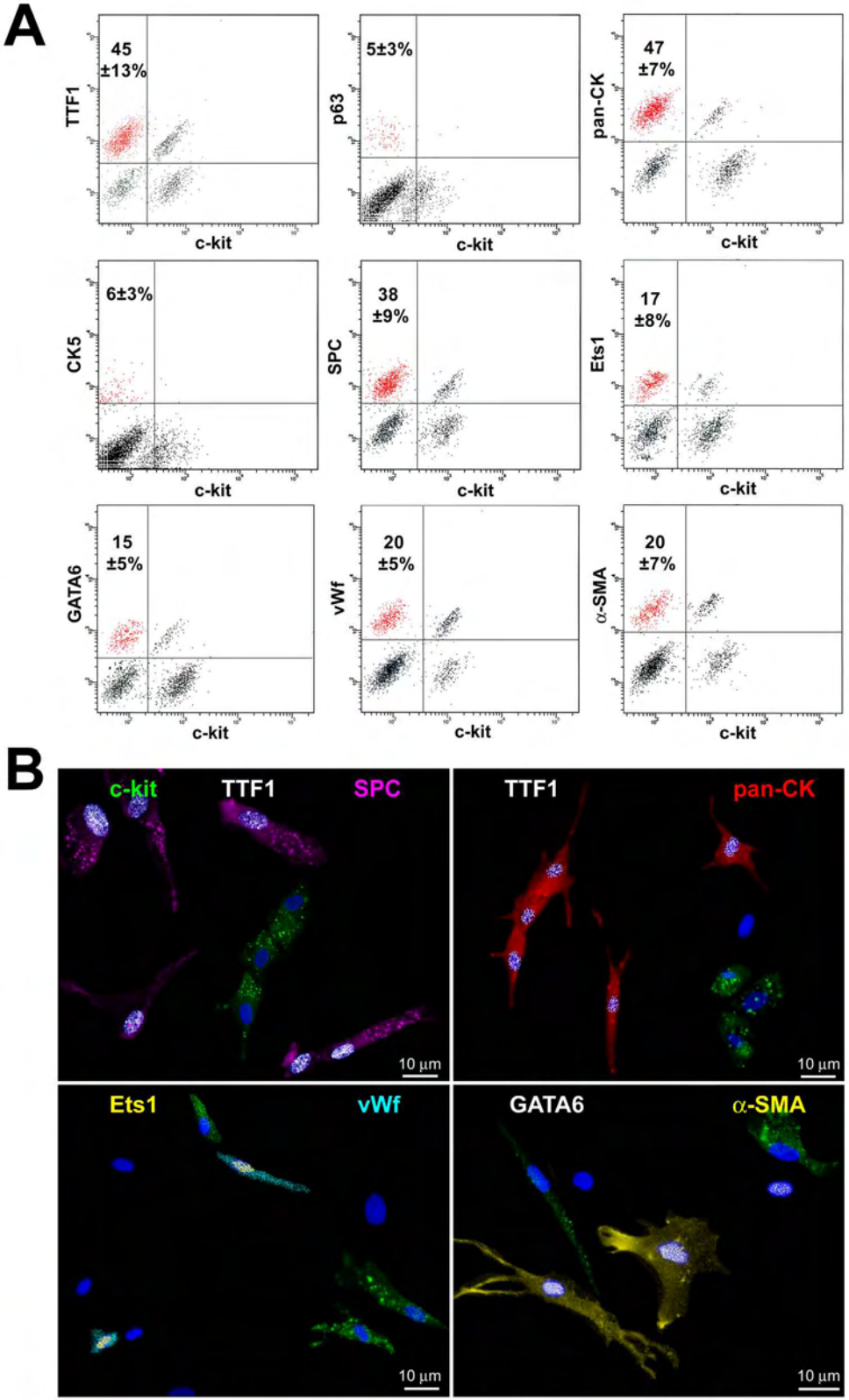

Supplementary Figure 4A, B

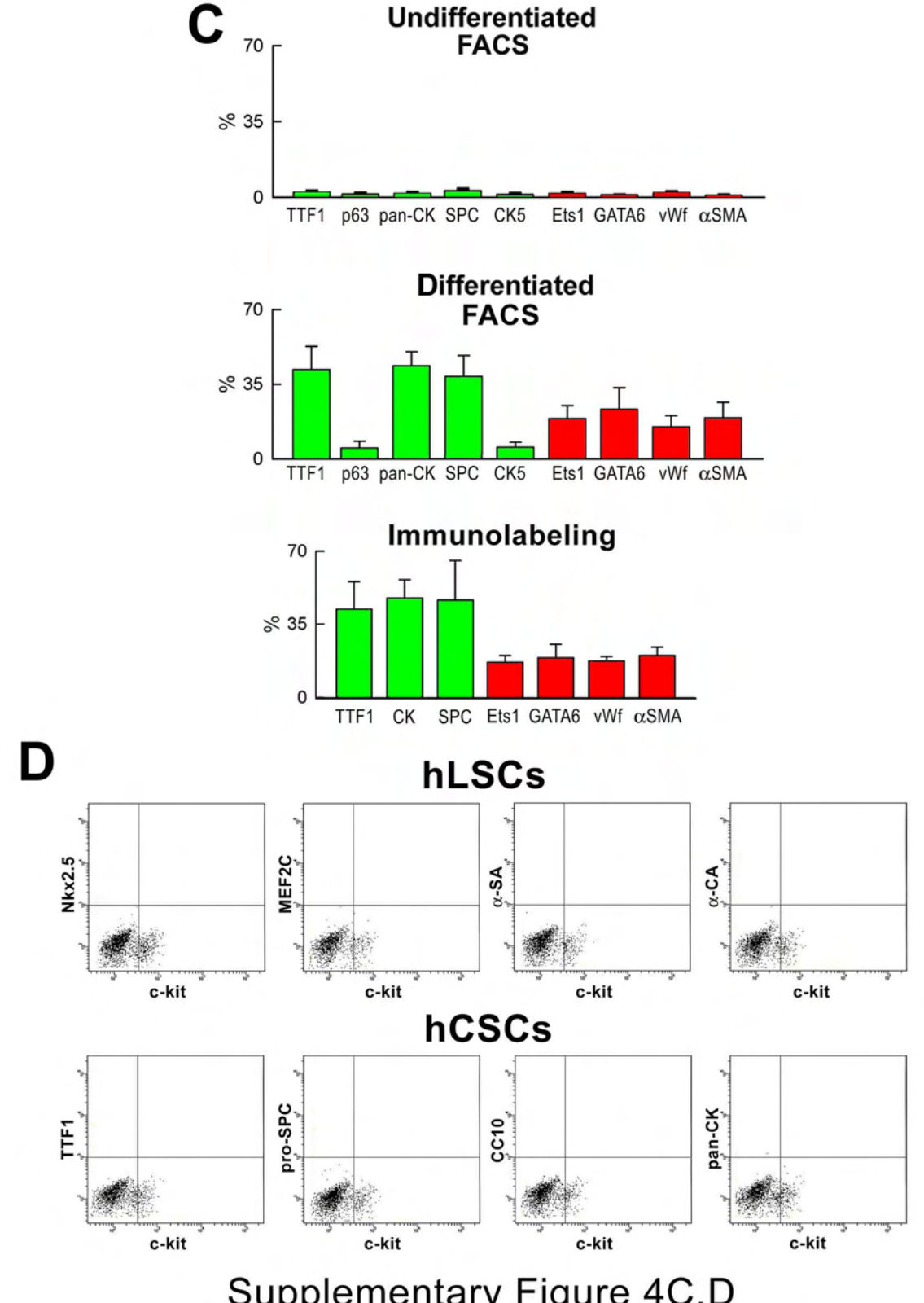

Supplementary Figure 4C,D

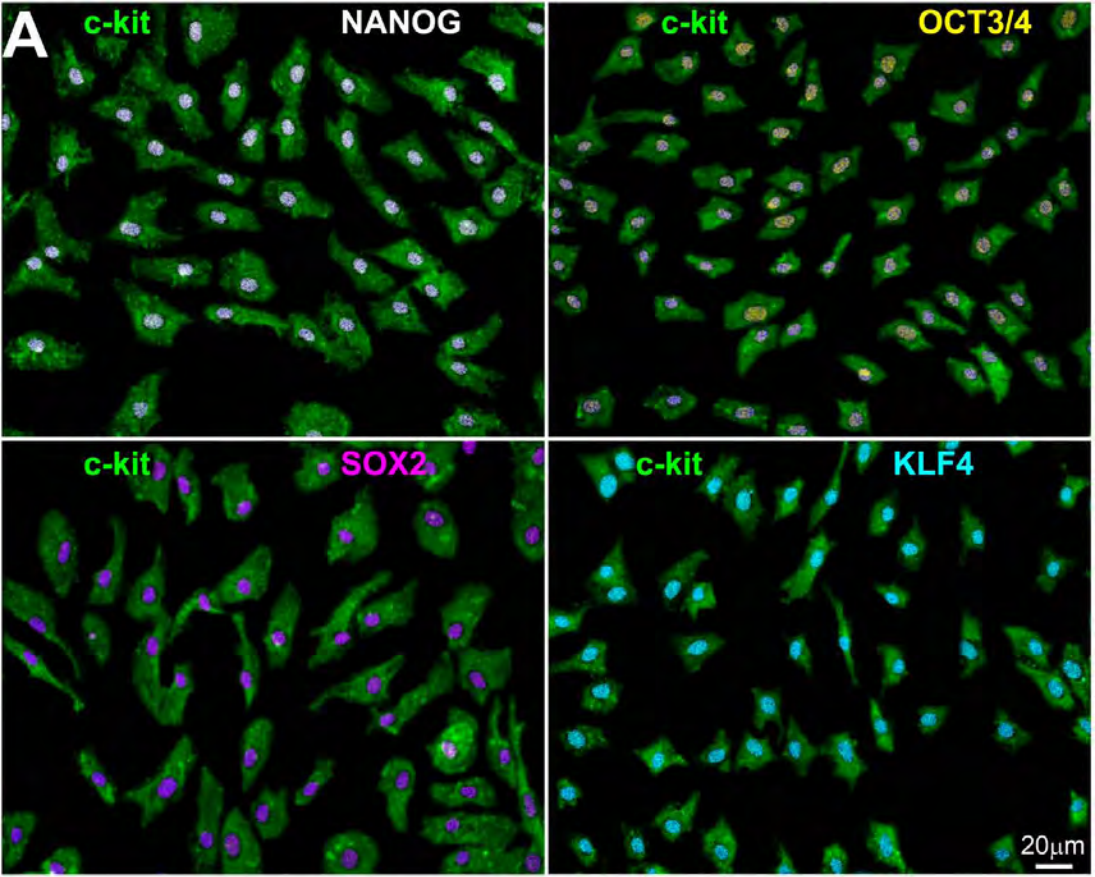

Supplementary Figure 5A

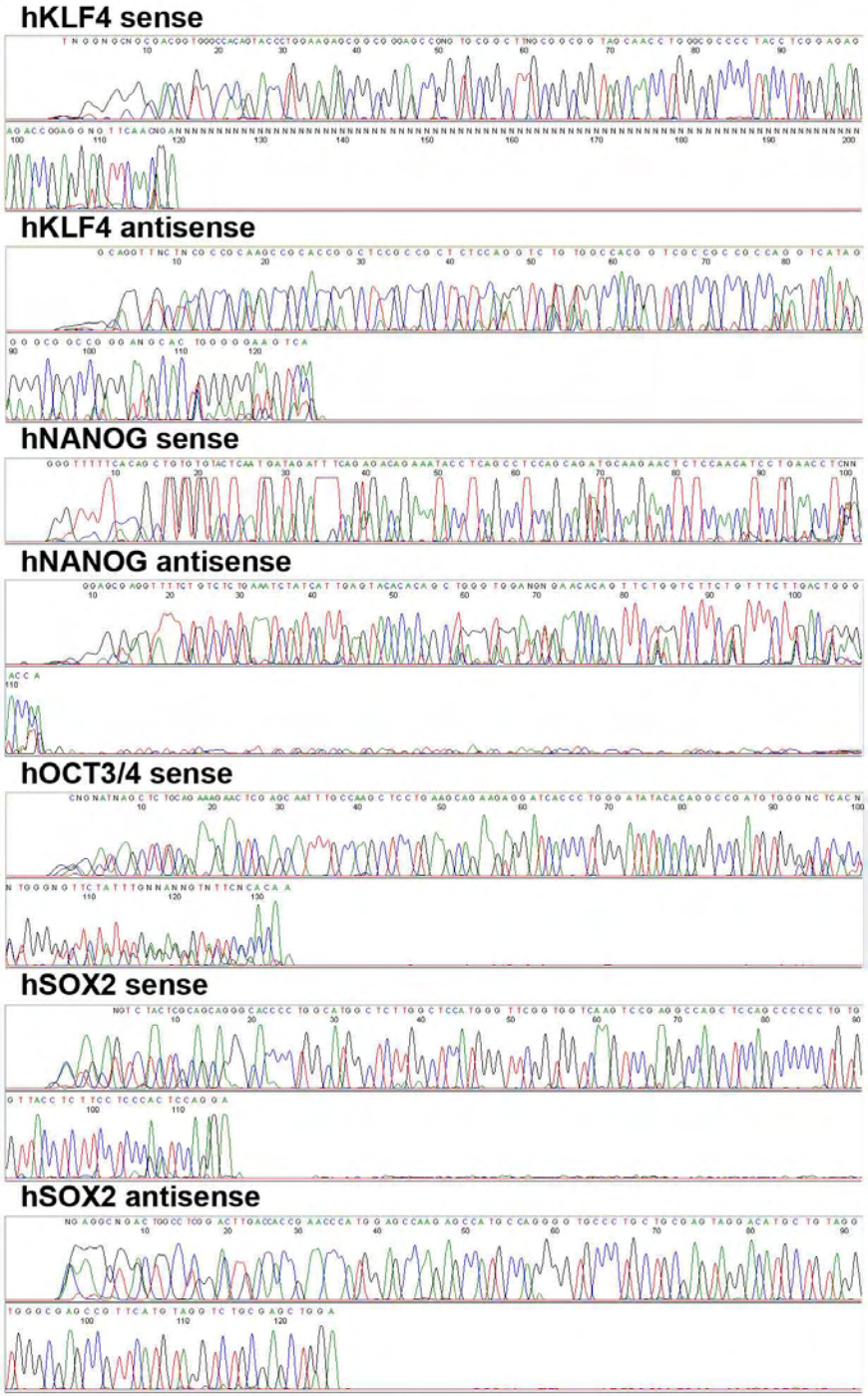

Supplementary Figure 5B

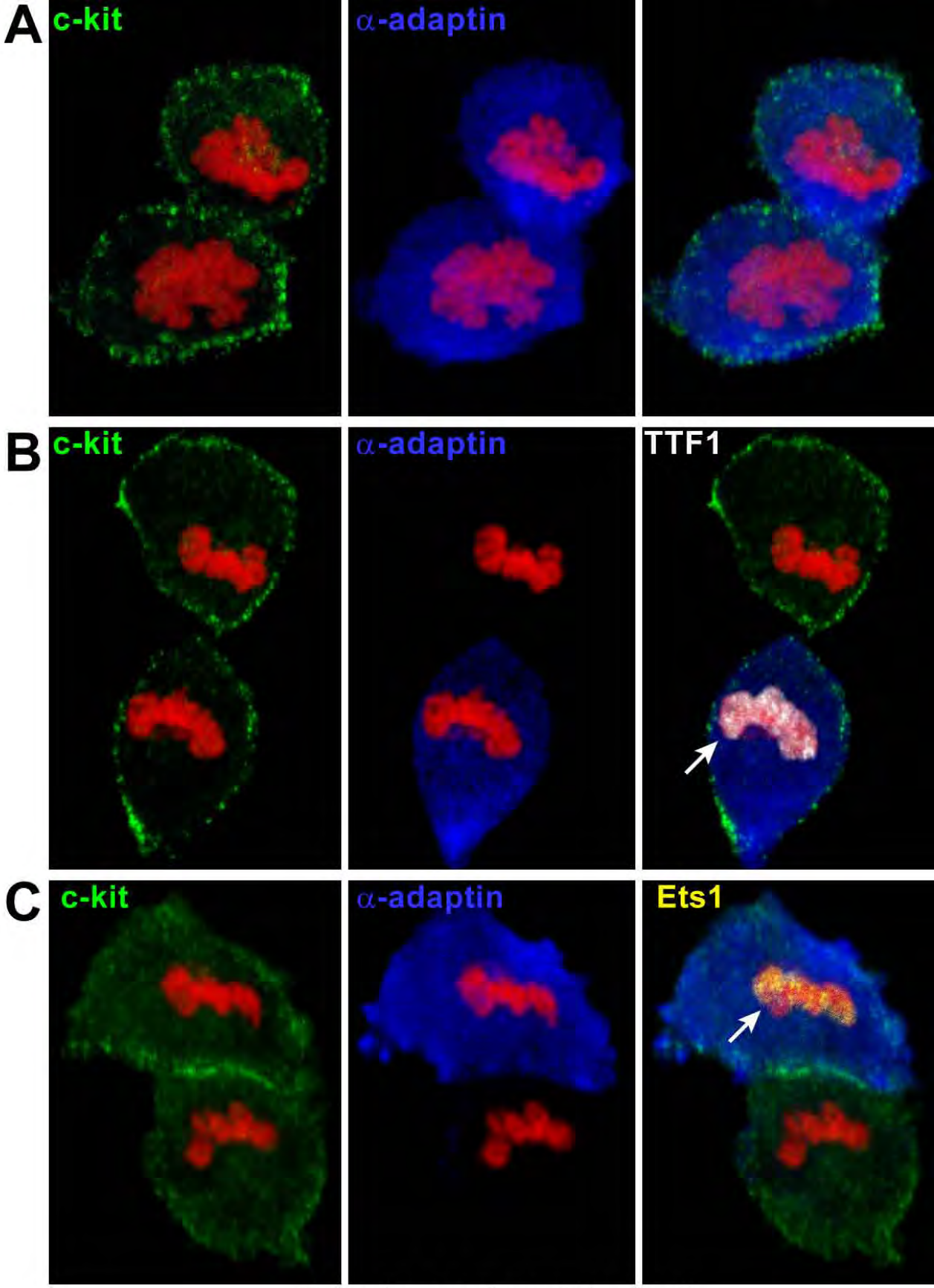

Supplementary Figure 6

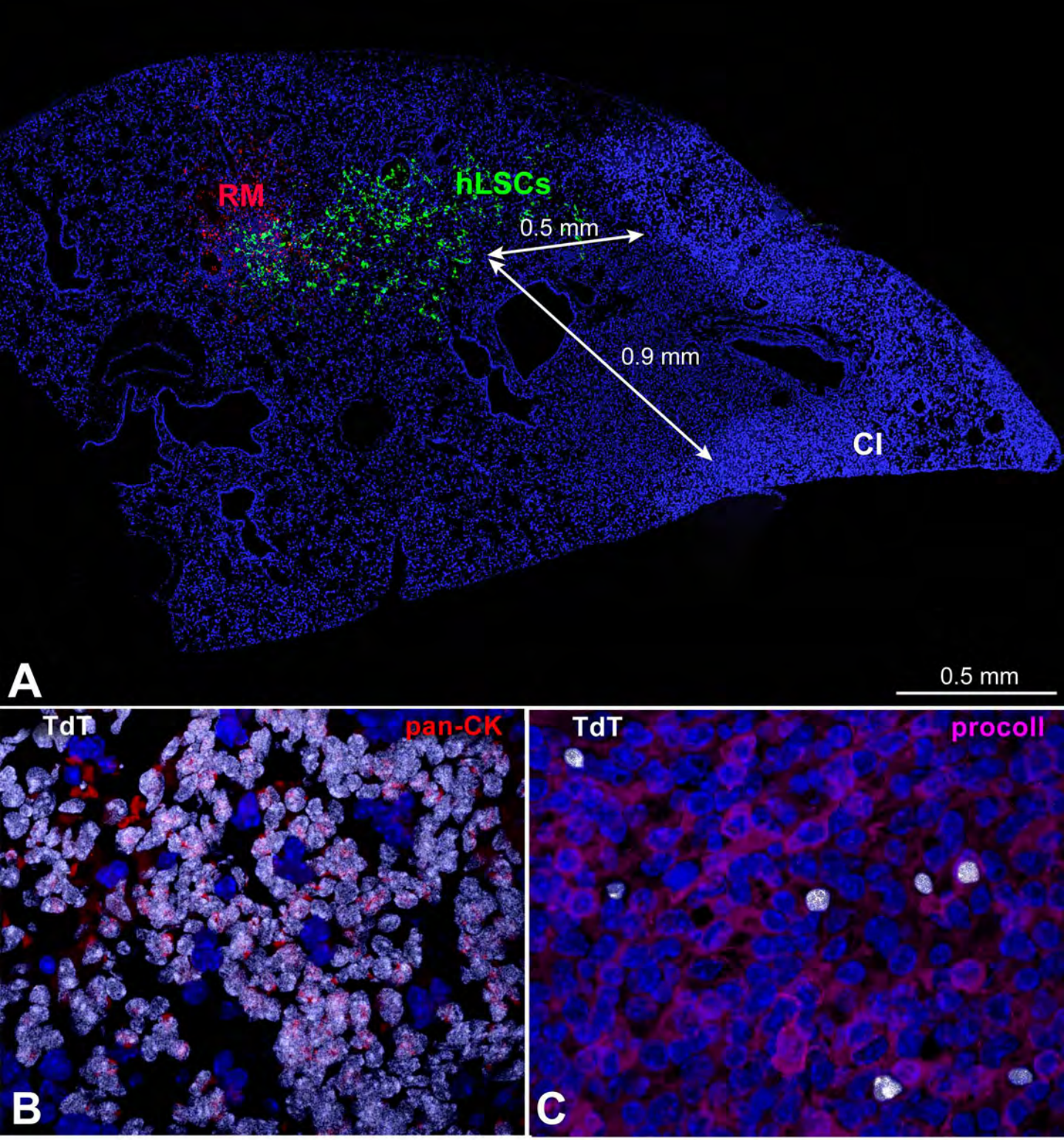

Supplementary Figure 7

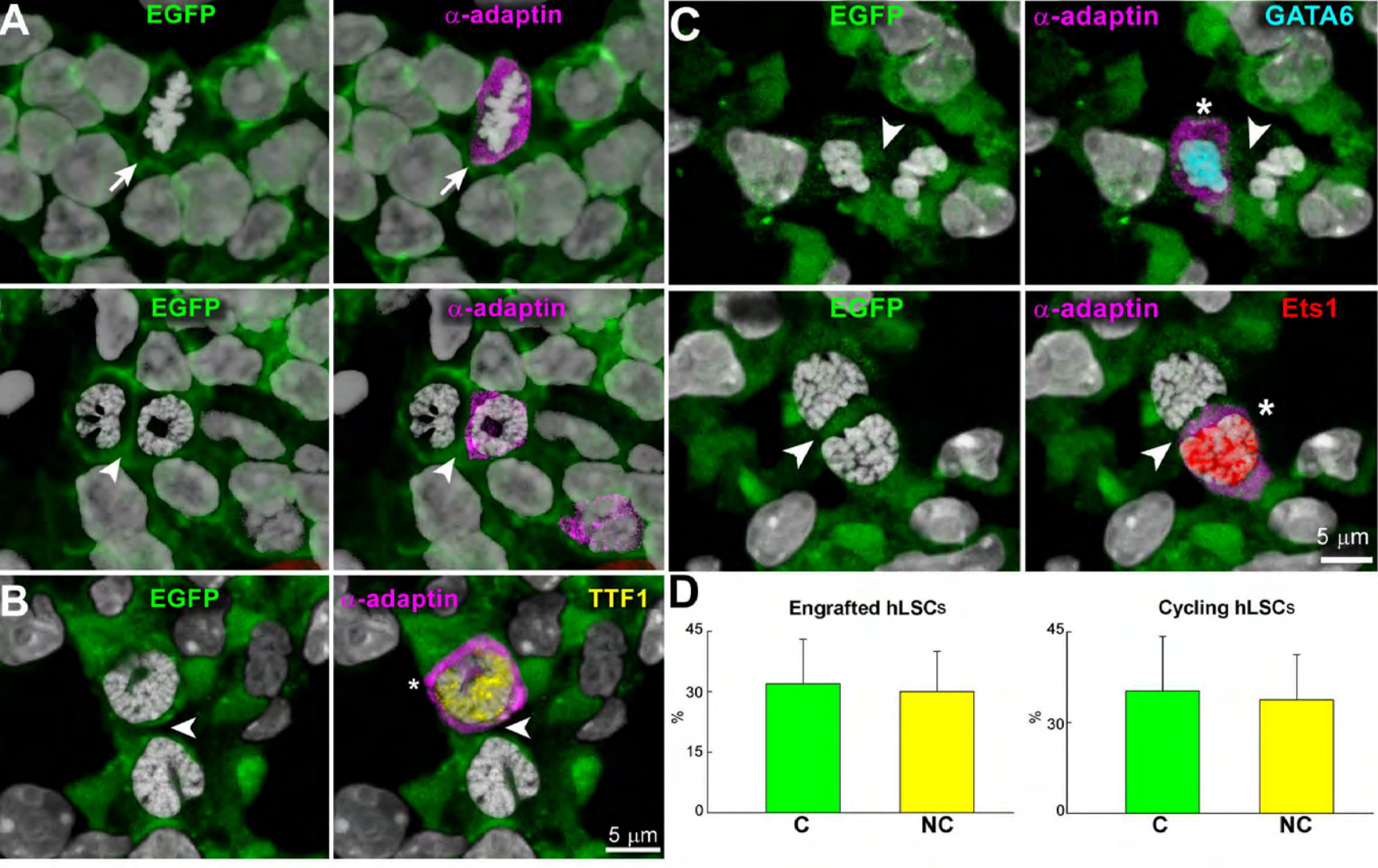

Supplementary Figure 8

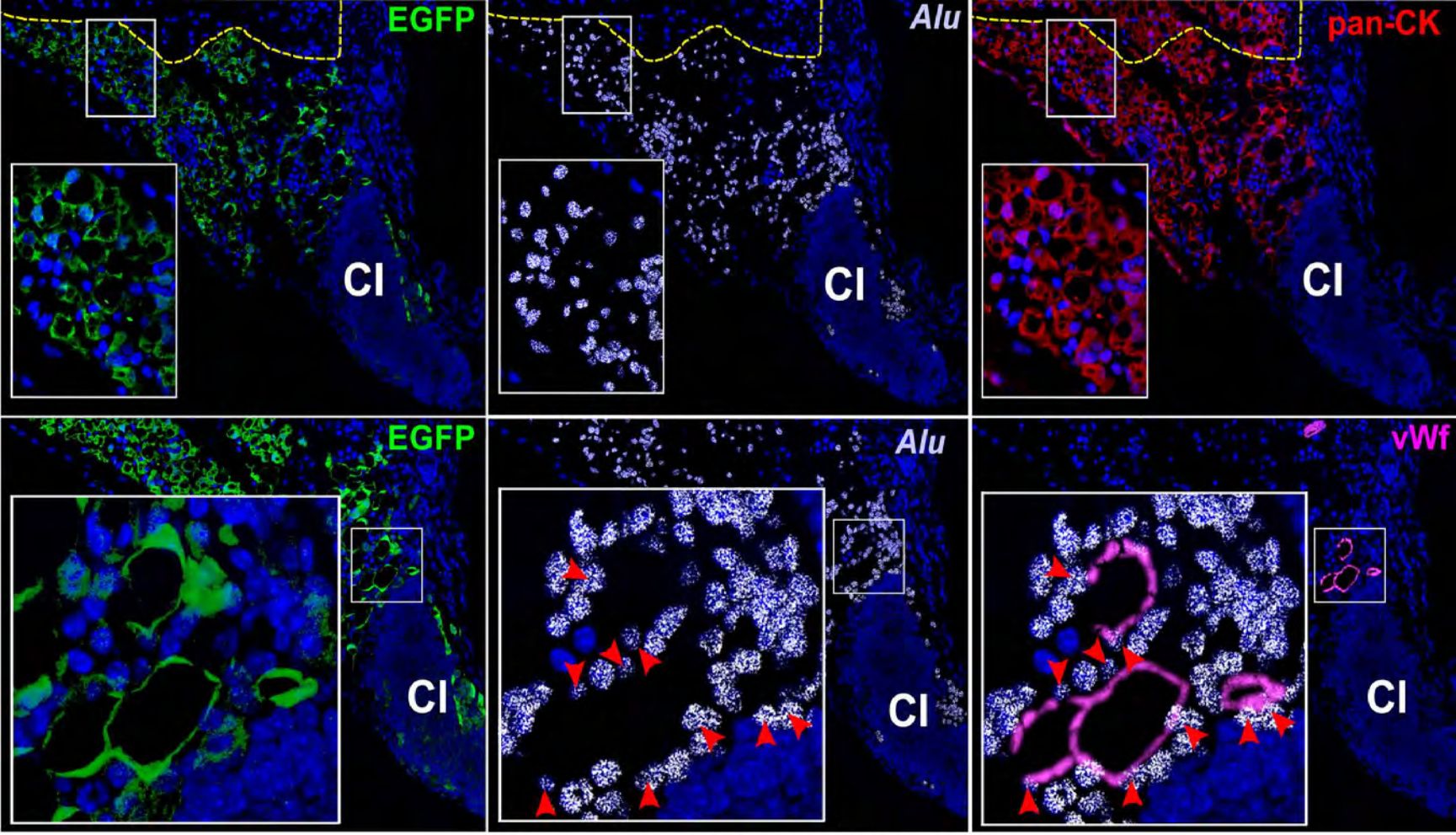

Supplementary Figure 9

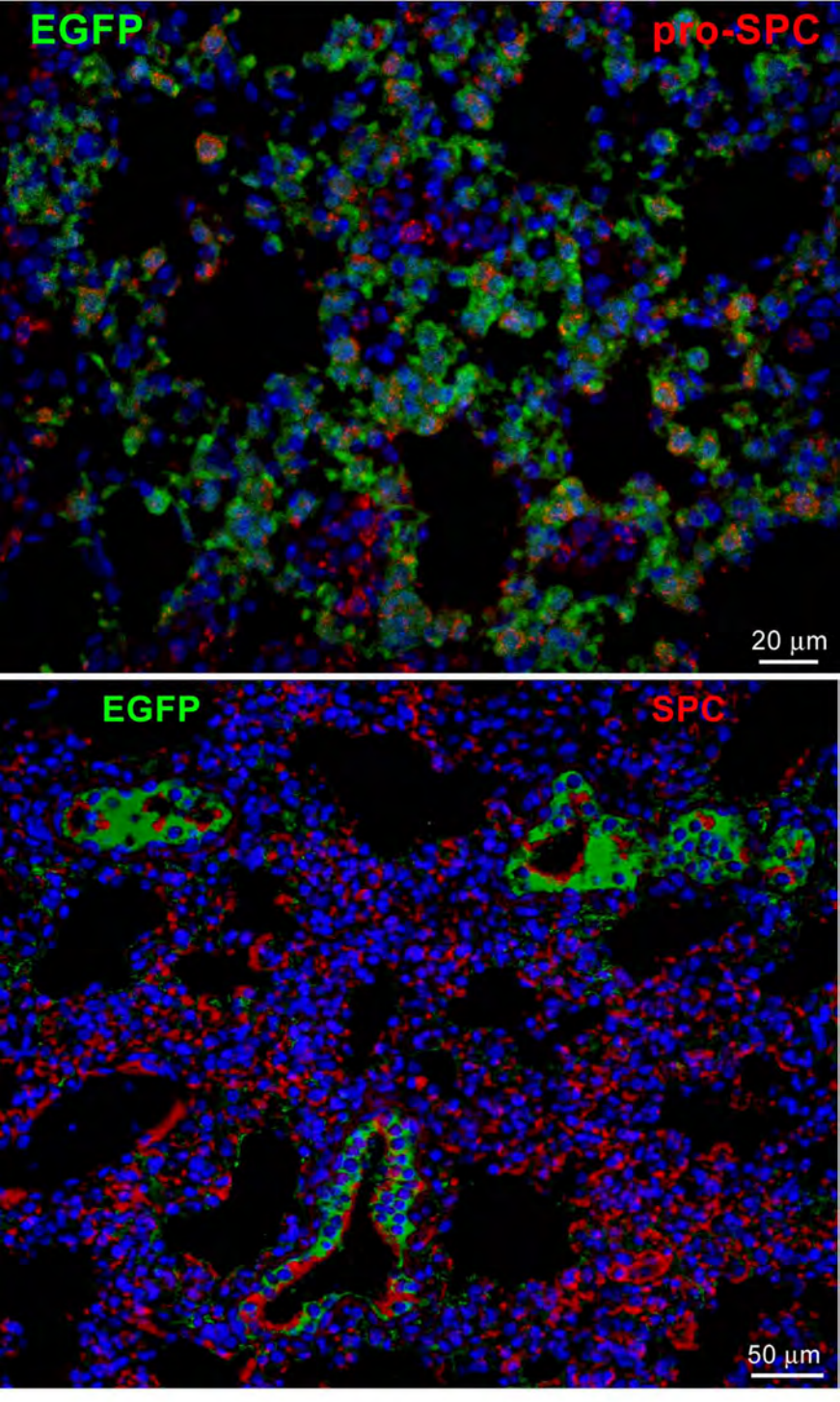

Supplementary Figure 10

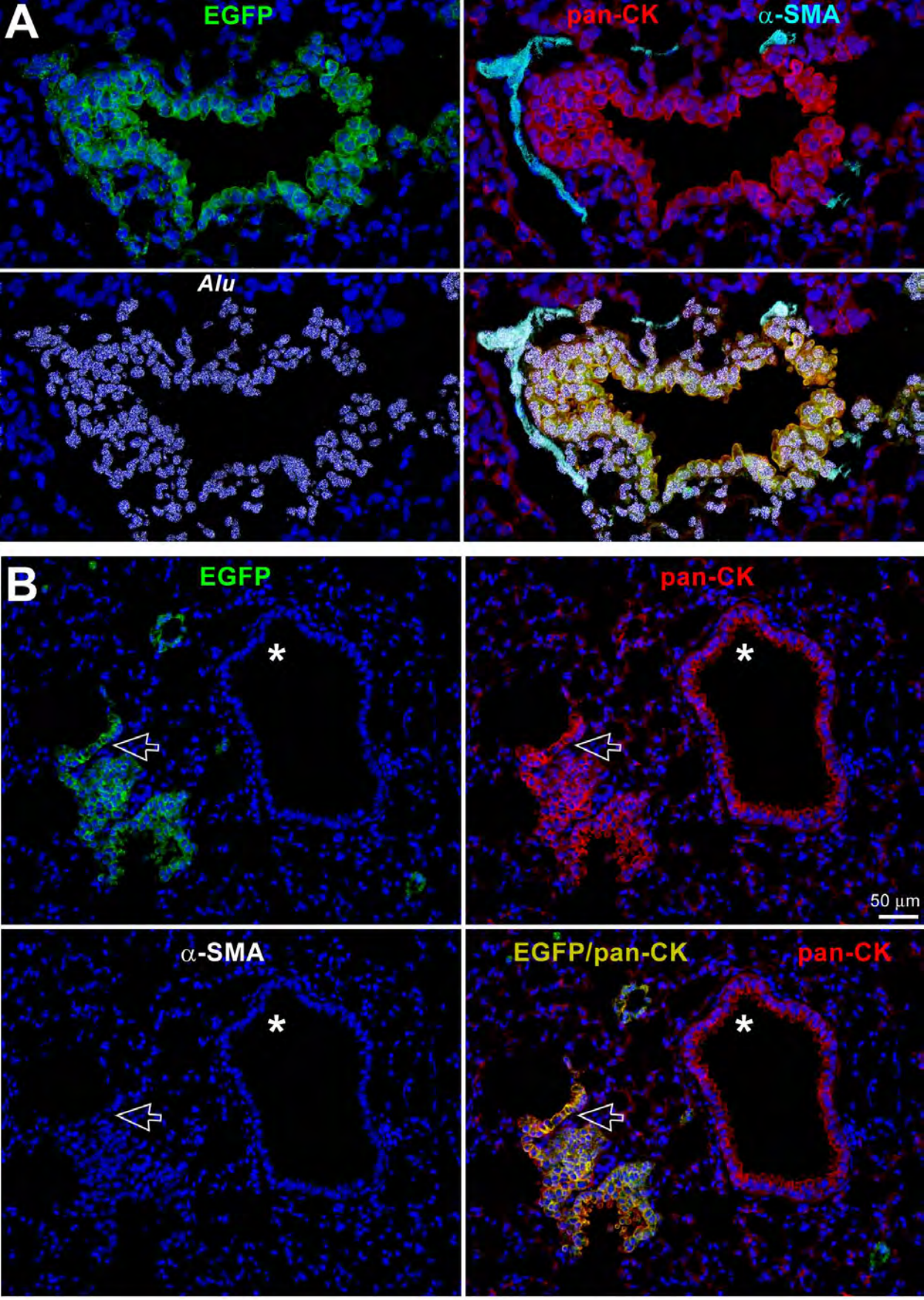

Supplementary Figure 11A, B

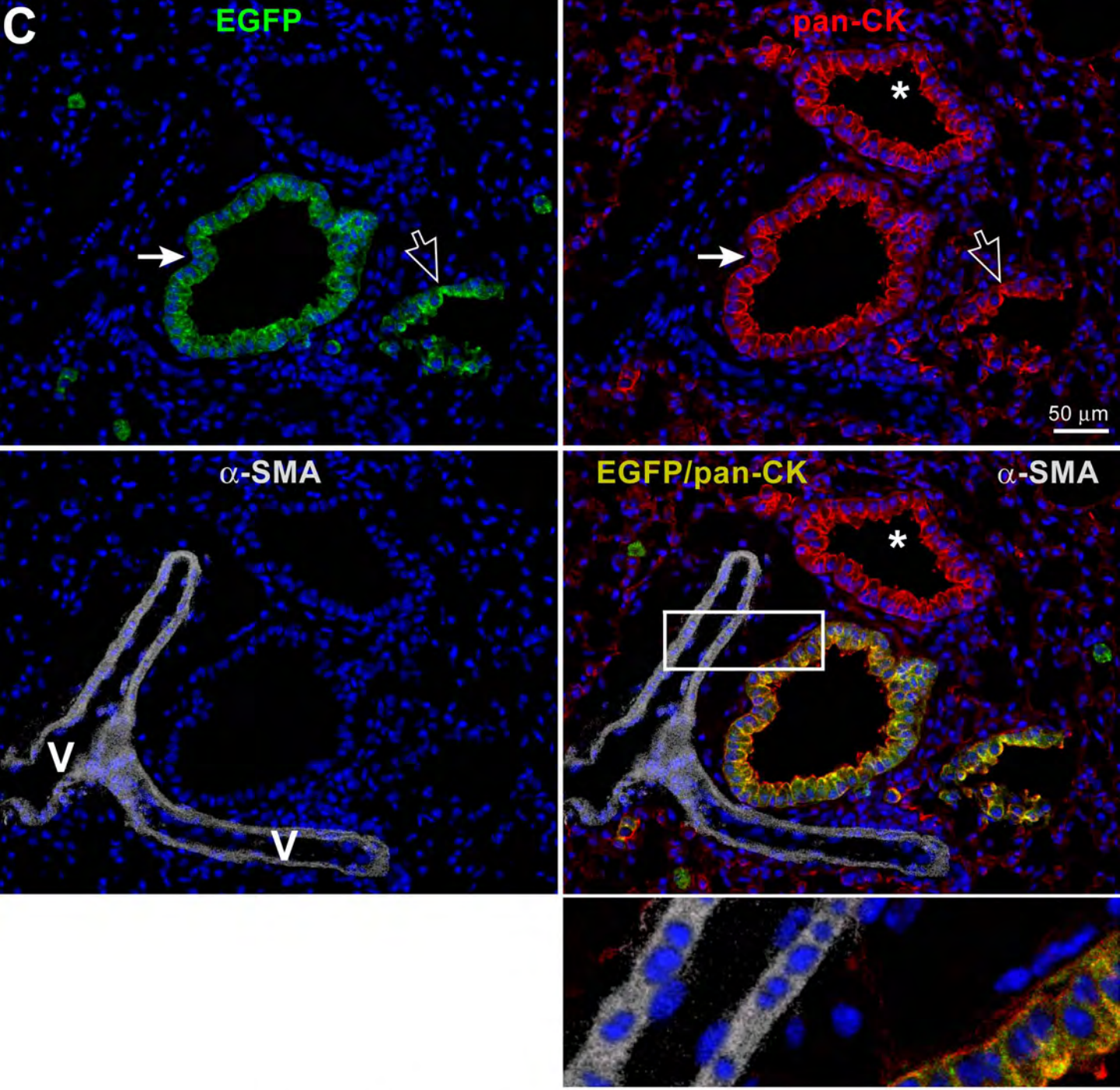

Supplementary Figure 11C

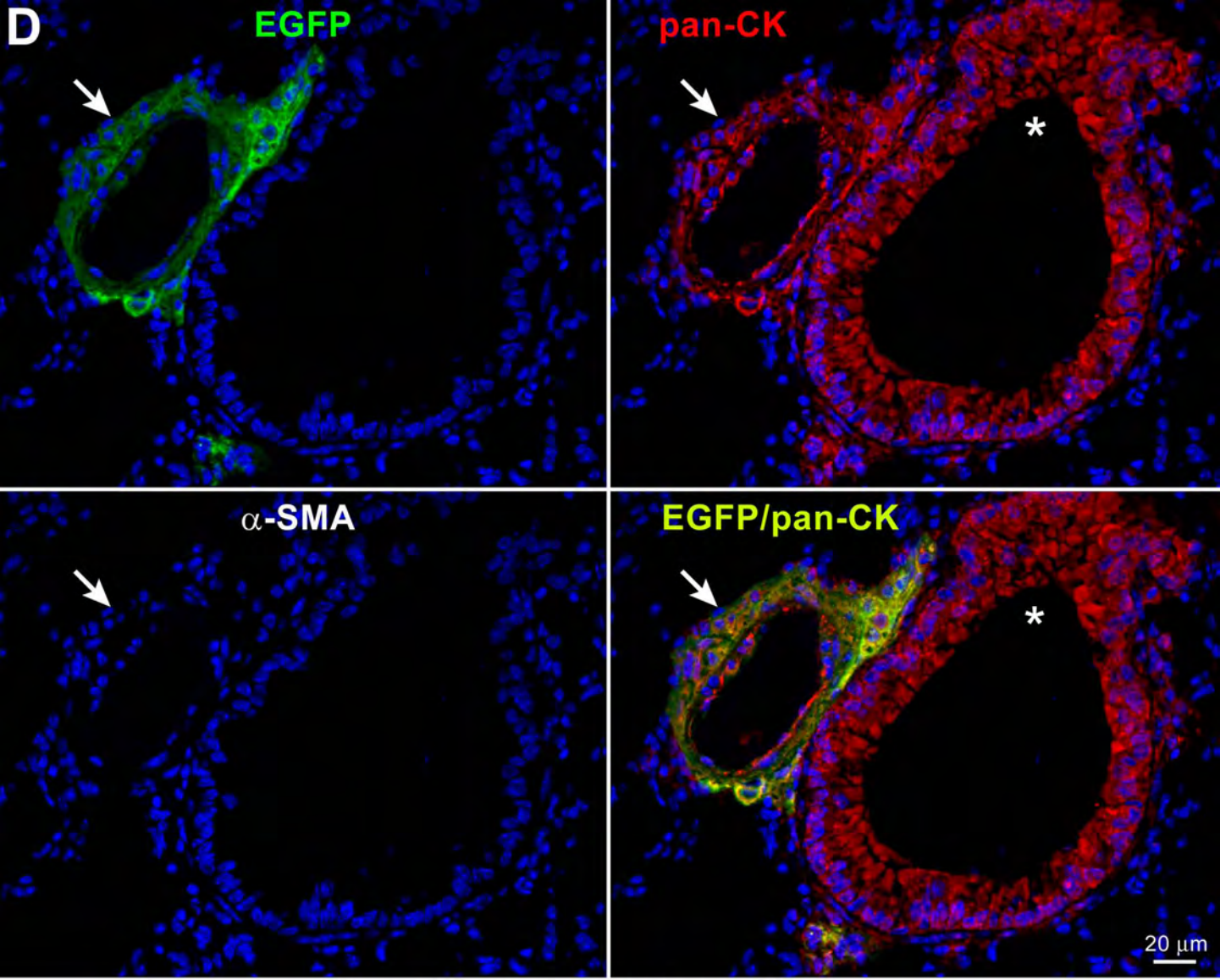

Supplementary Figure 11D

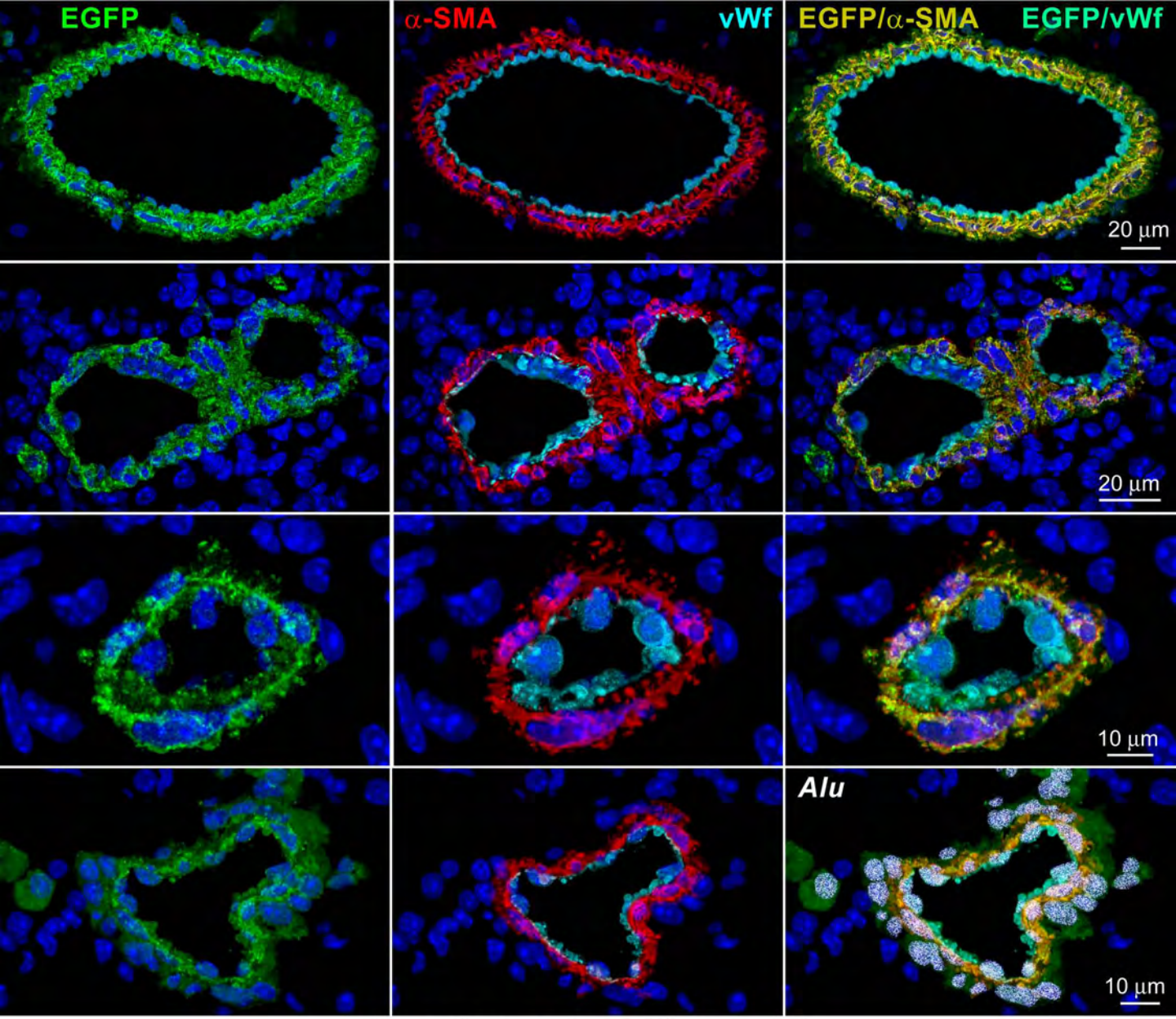

Supplementary Figure 12

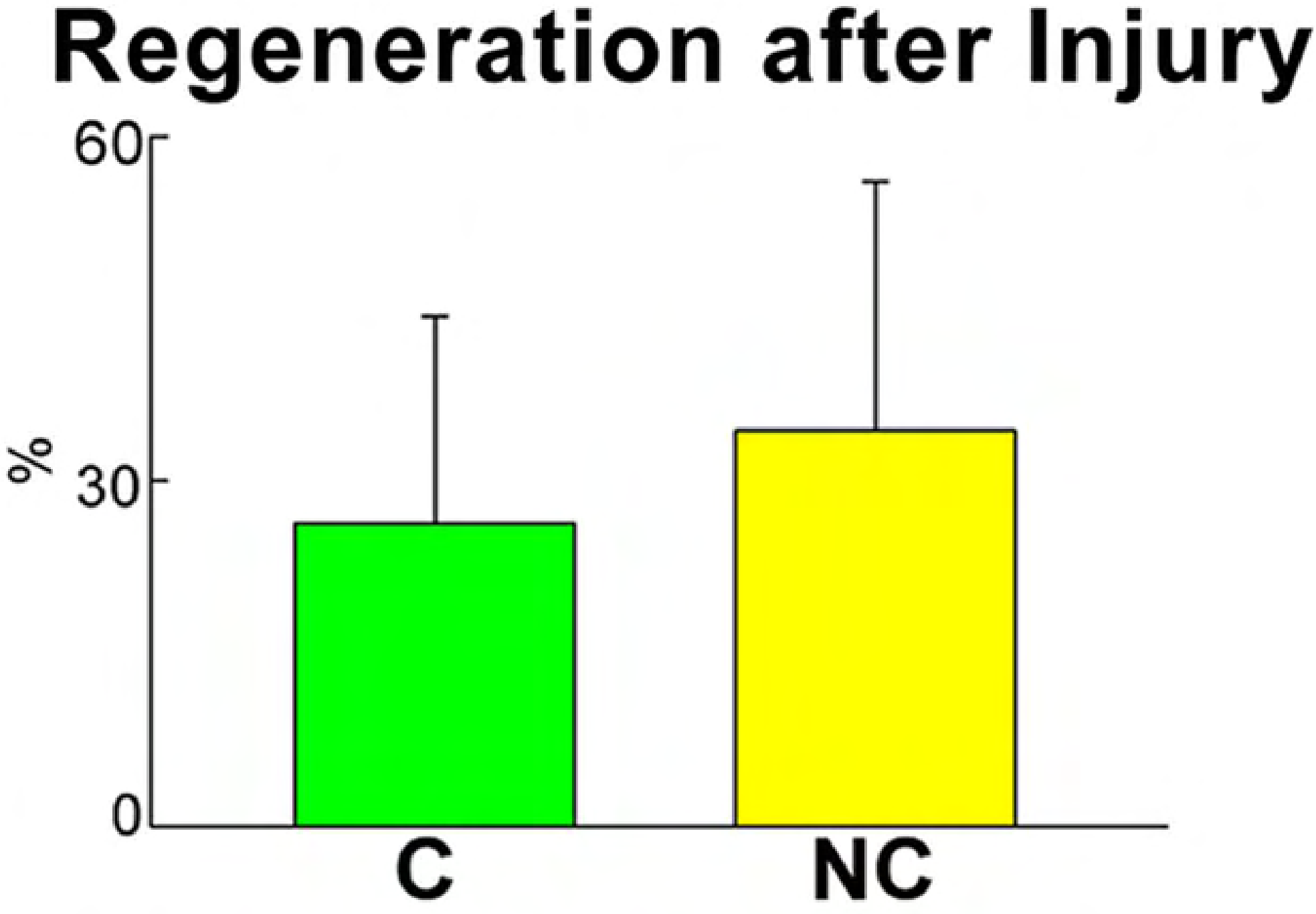

Supplementary Figure 13

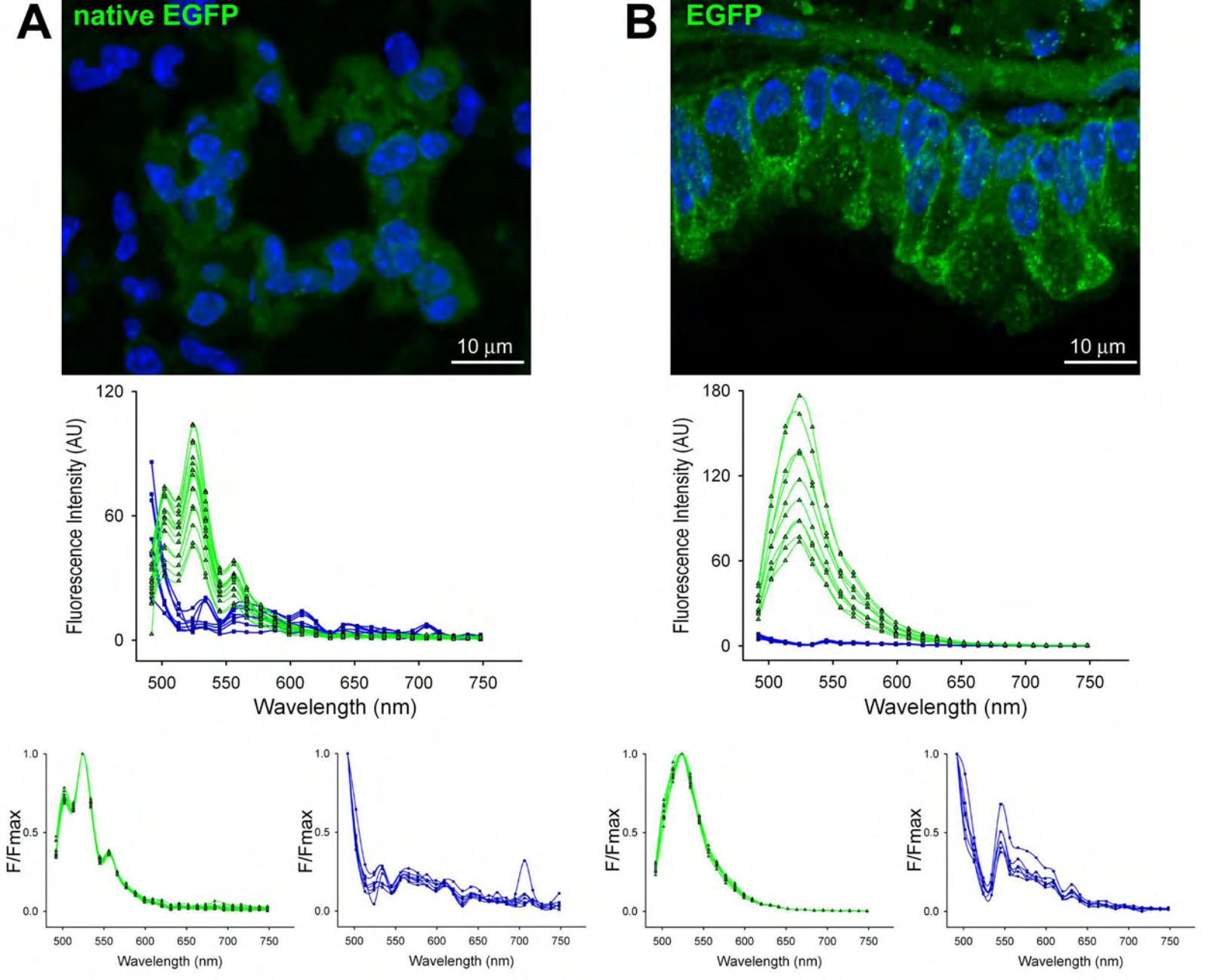

Supplementary Figure 14A,B

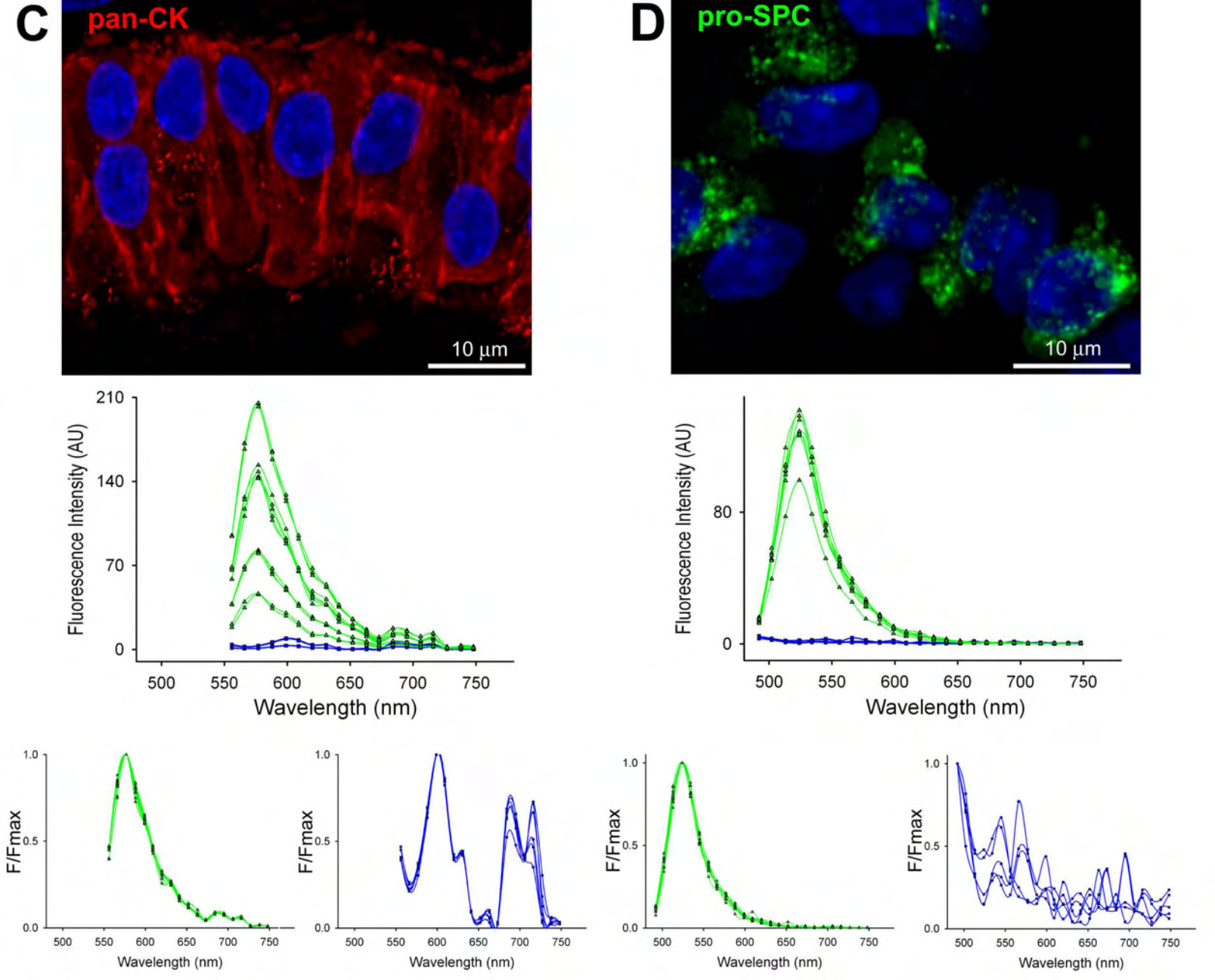

Supplementary Figure 14C,D

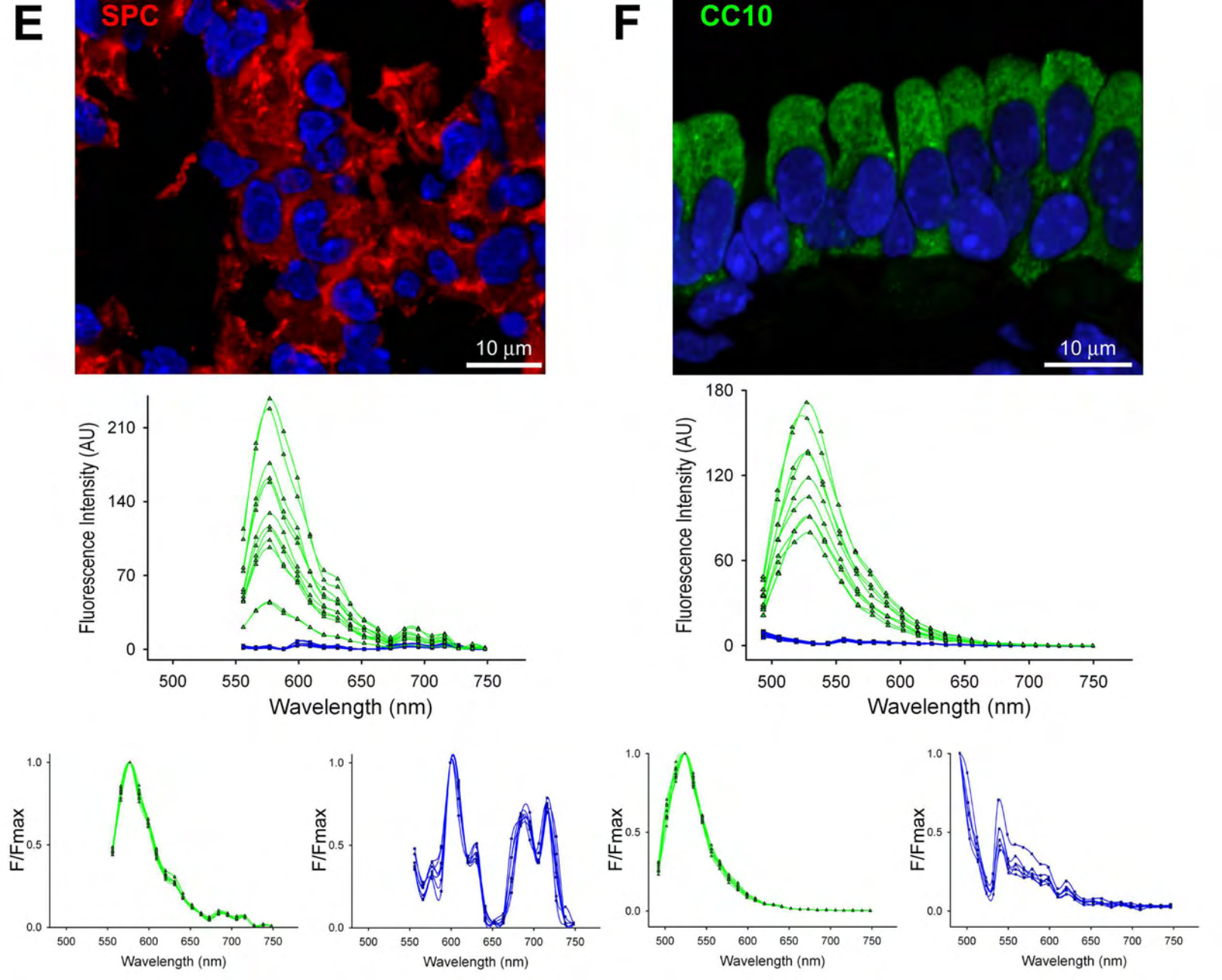

Supplementary Figure 14E,F

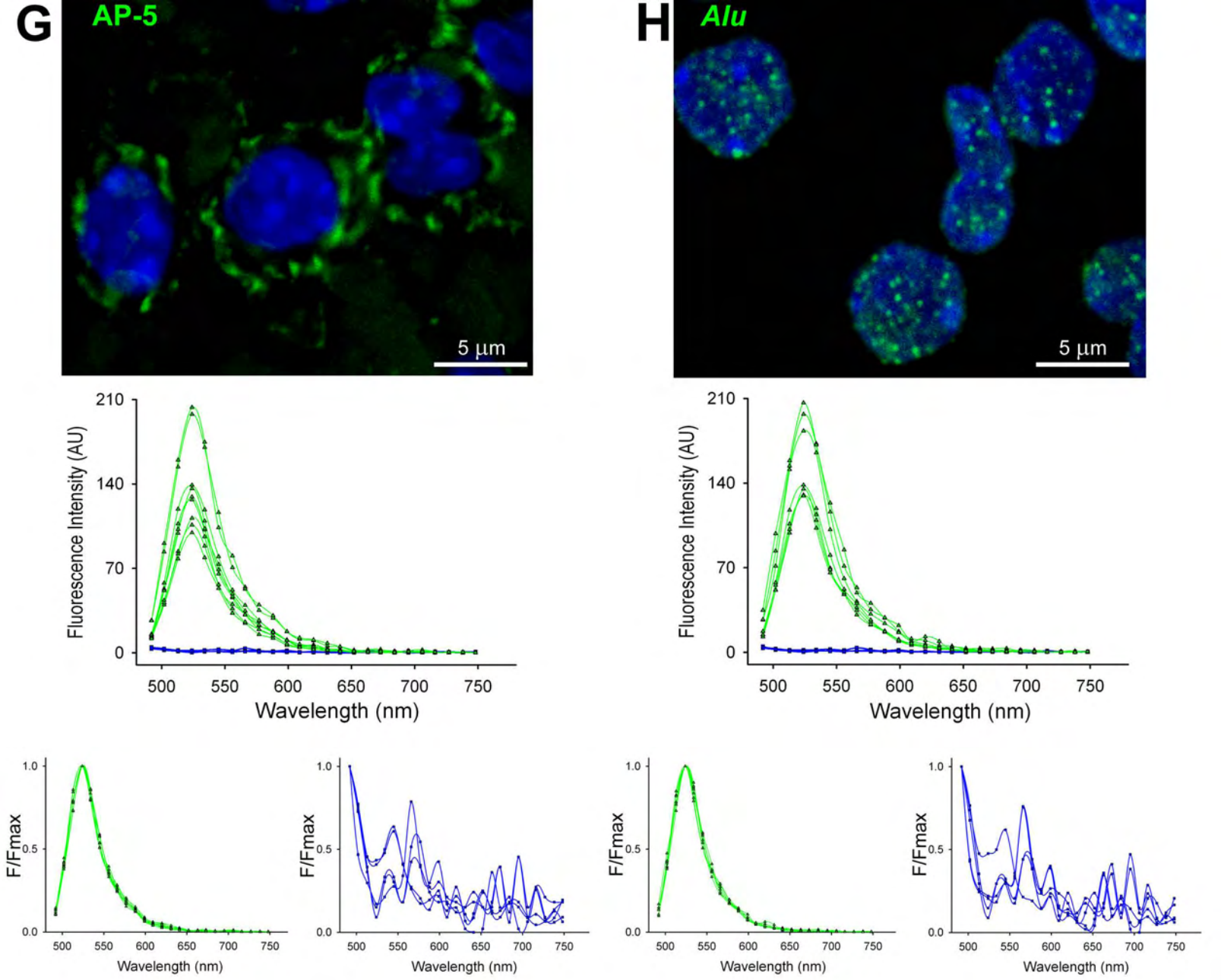

Supplementary Figure 14G,H

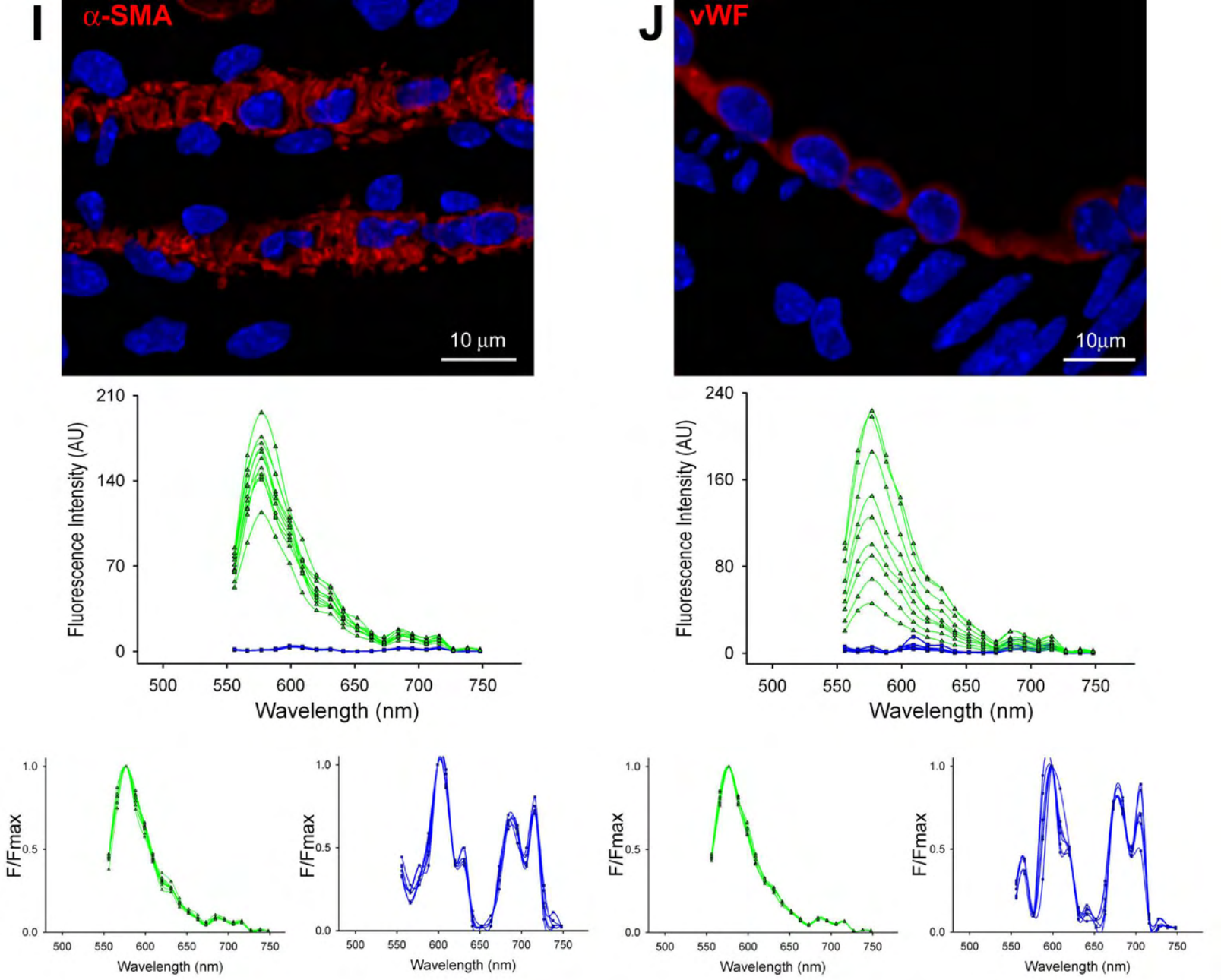

Supplementary Figure 14I, J

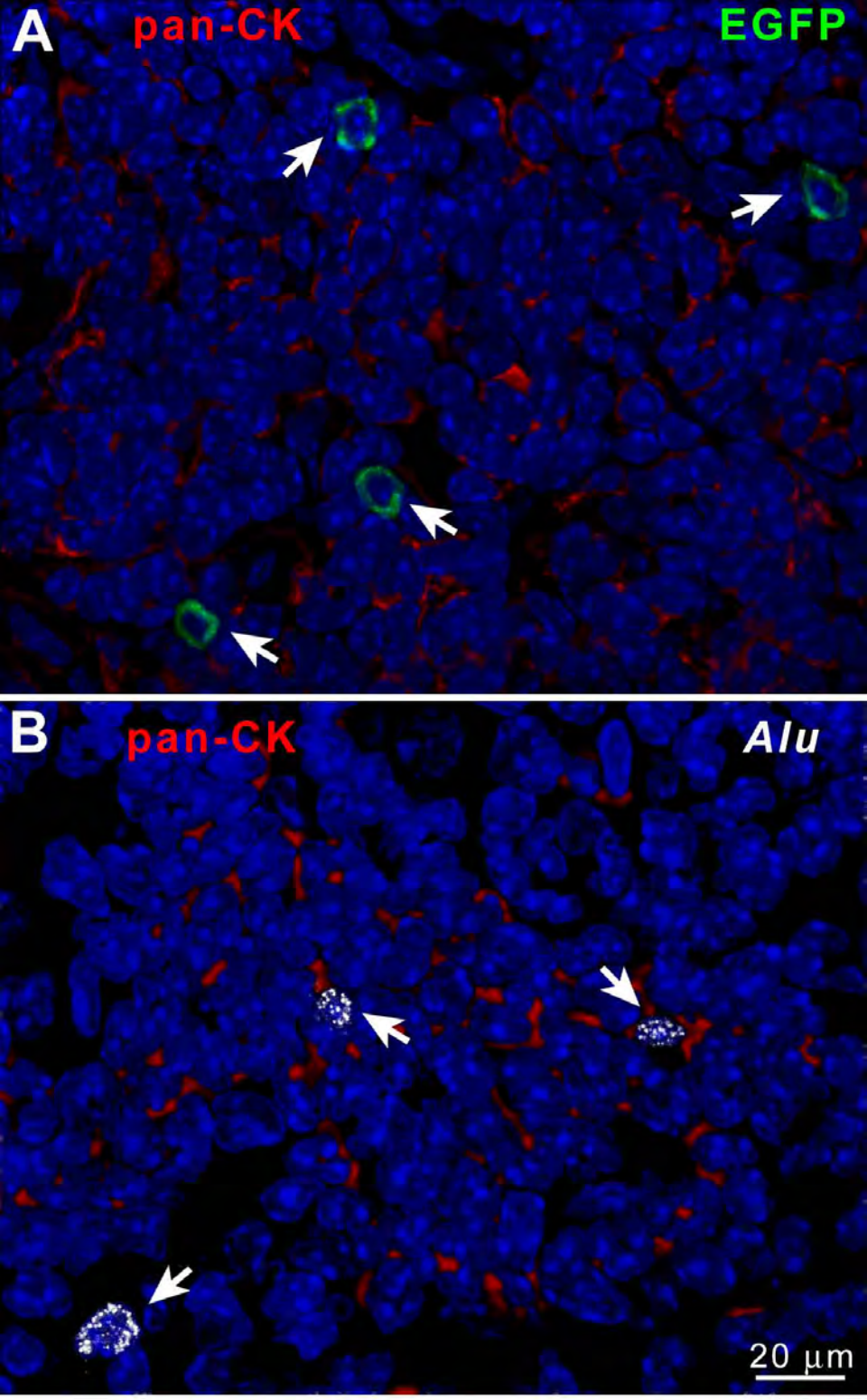

Supplementary Figure 15

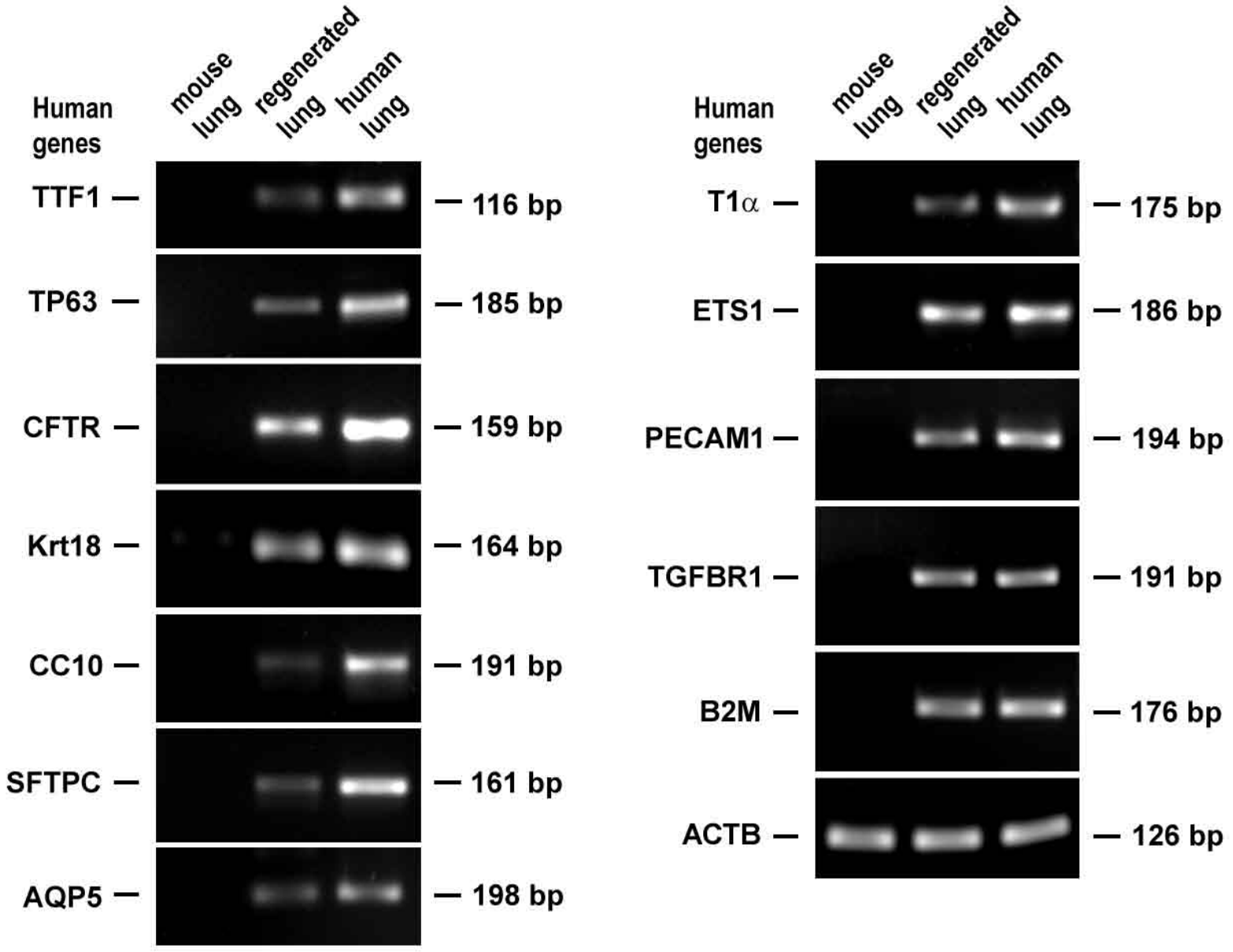

Supplementary Figure 16A

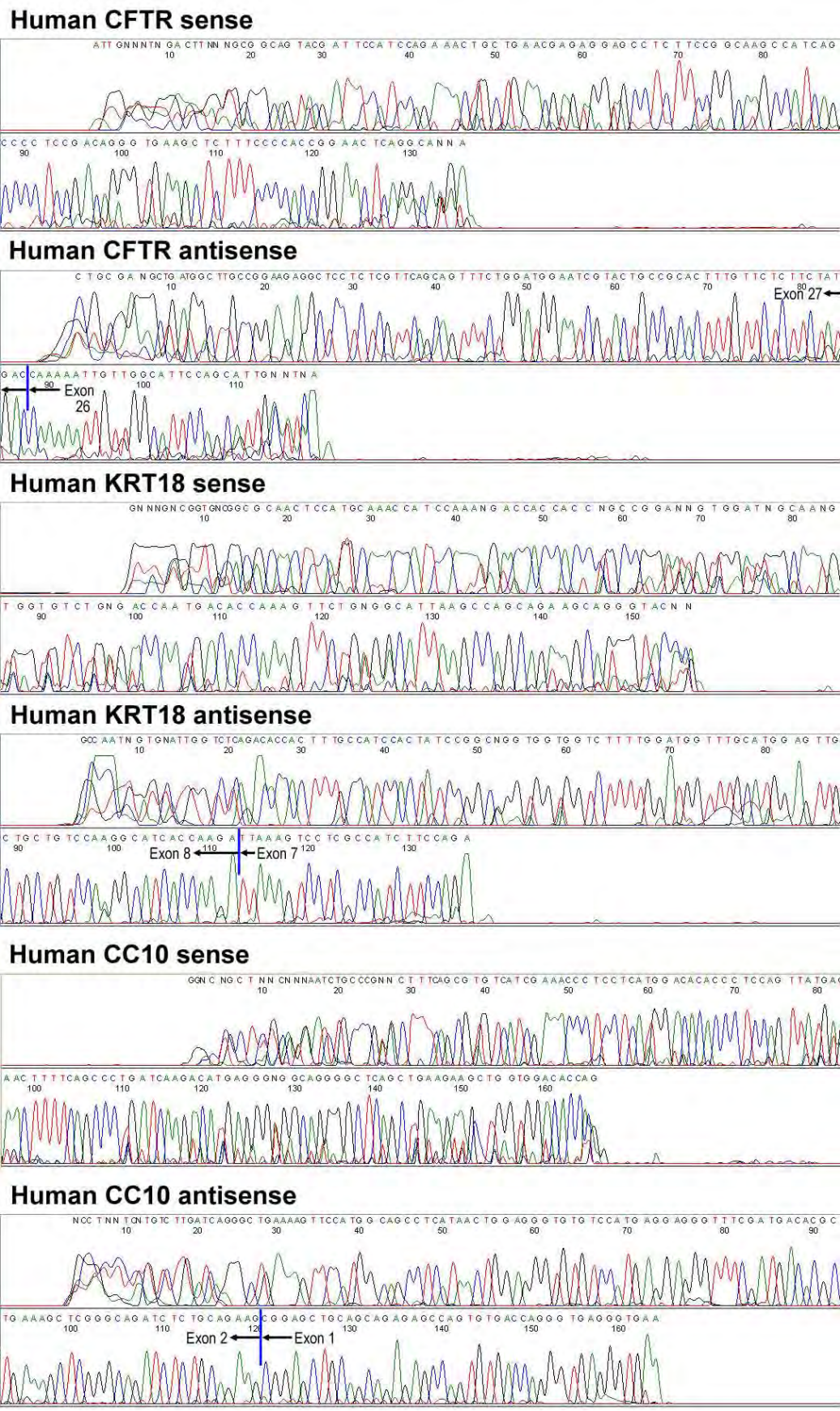

Supplementary Figure 16B part 1

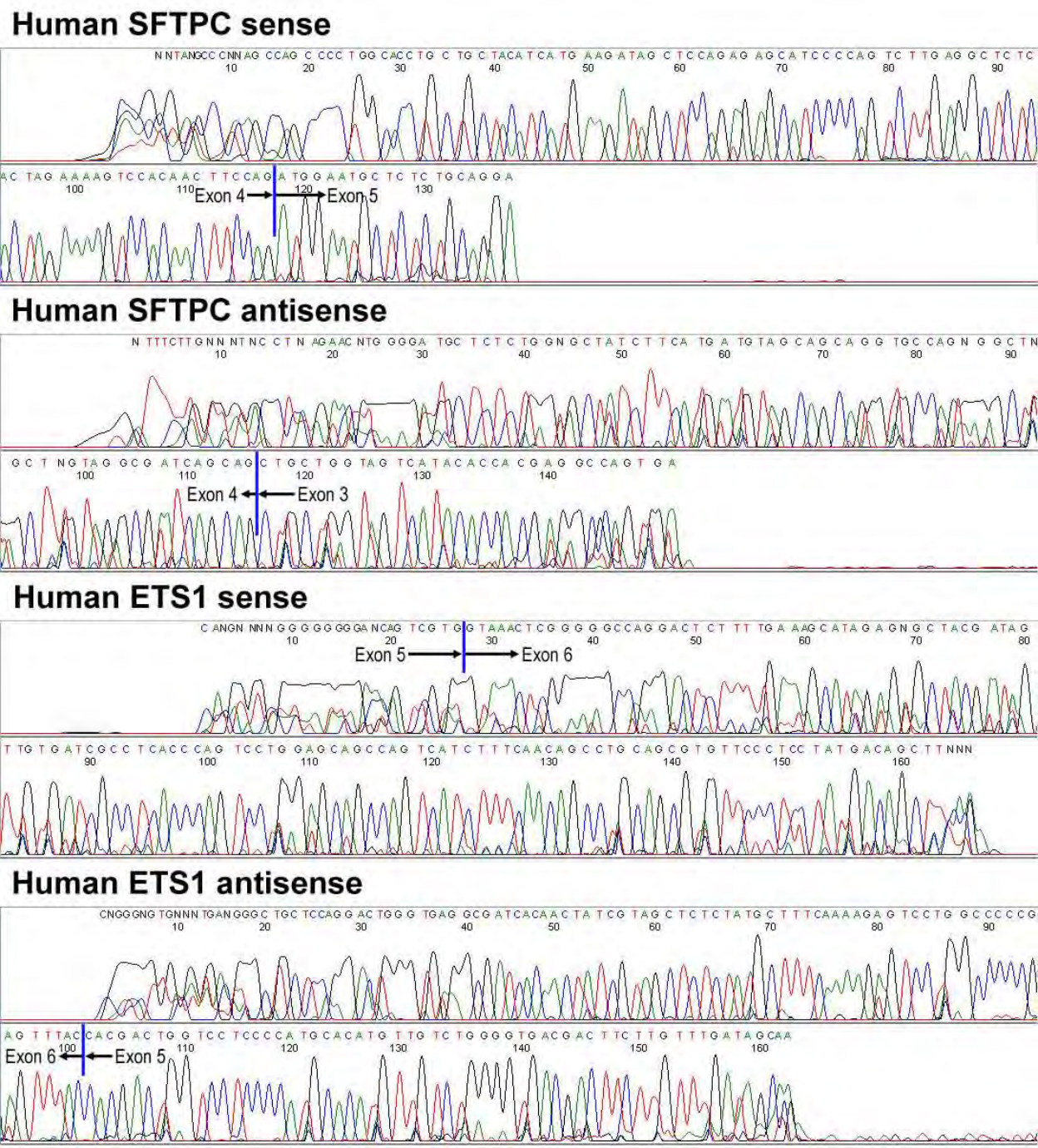

Supplementary Figure 16B part 2

Human Tp63 antisense

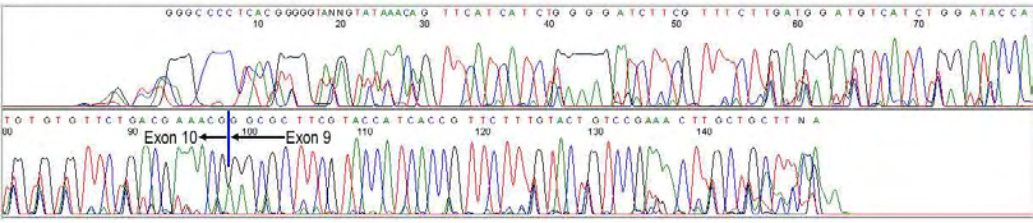

Human TTF1 sense

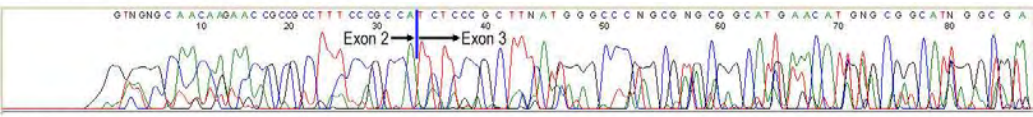

Human TTF1 antisense

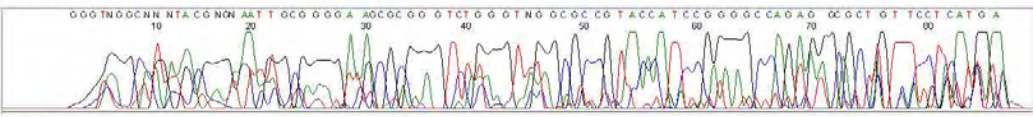

Human Aqp5 sense

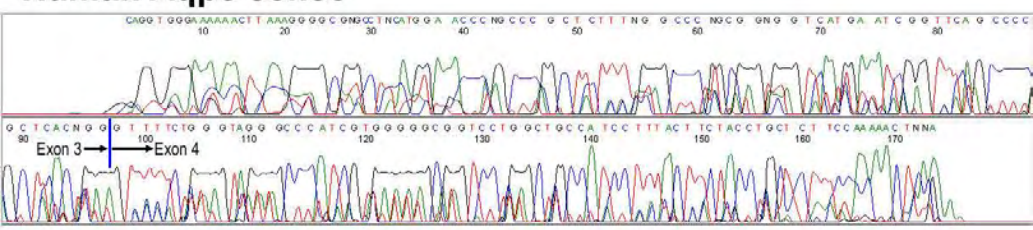

Human Aqp5 antisense

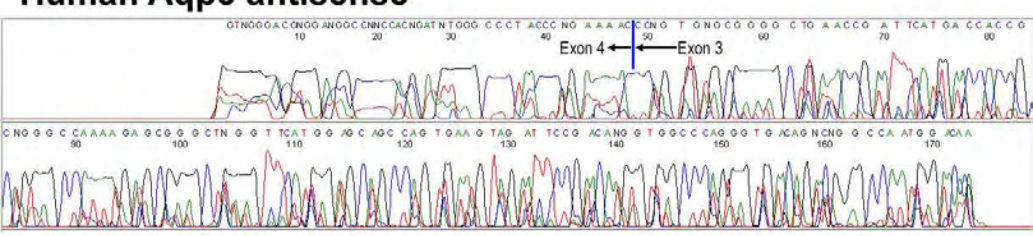

Human Pdpn antisense

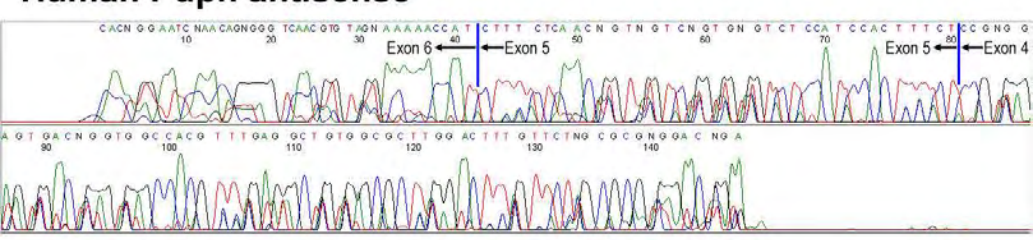

Human PECAM1 antisense

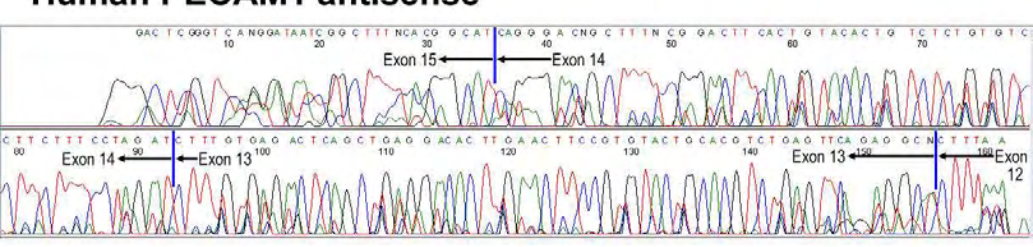

Supplementary Figure 16B part 3

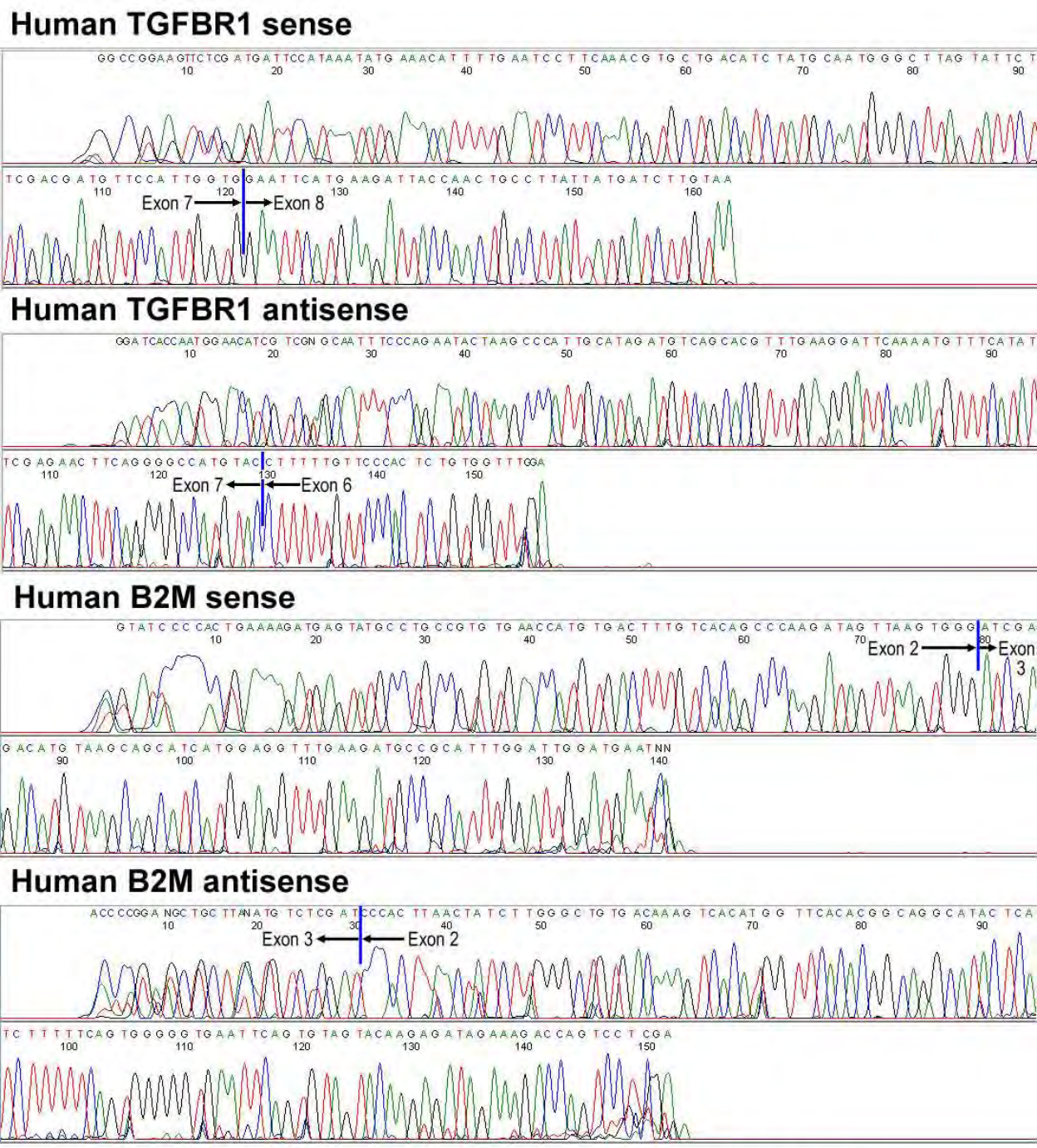

Supplementary Figure 16B part 4

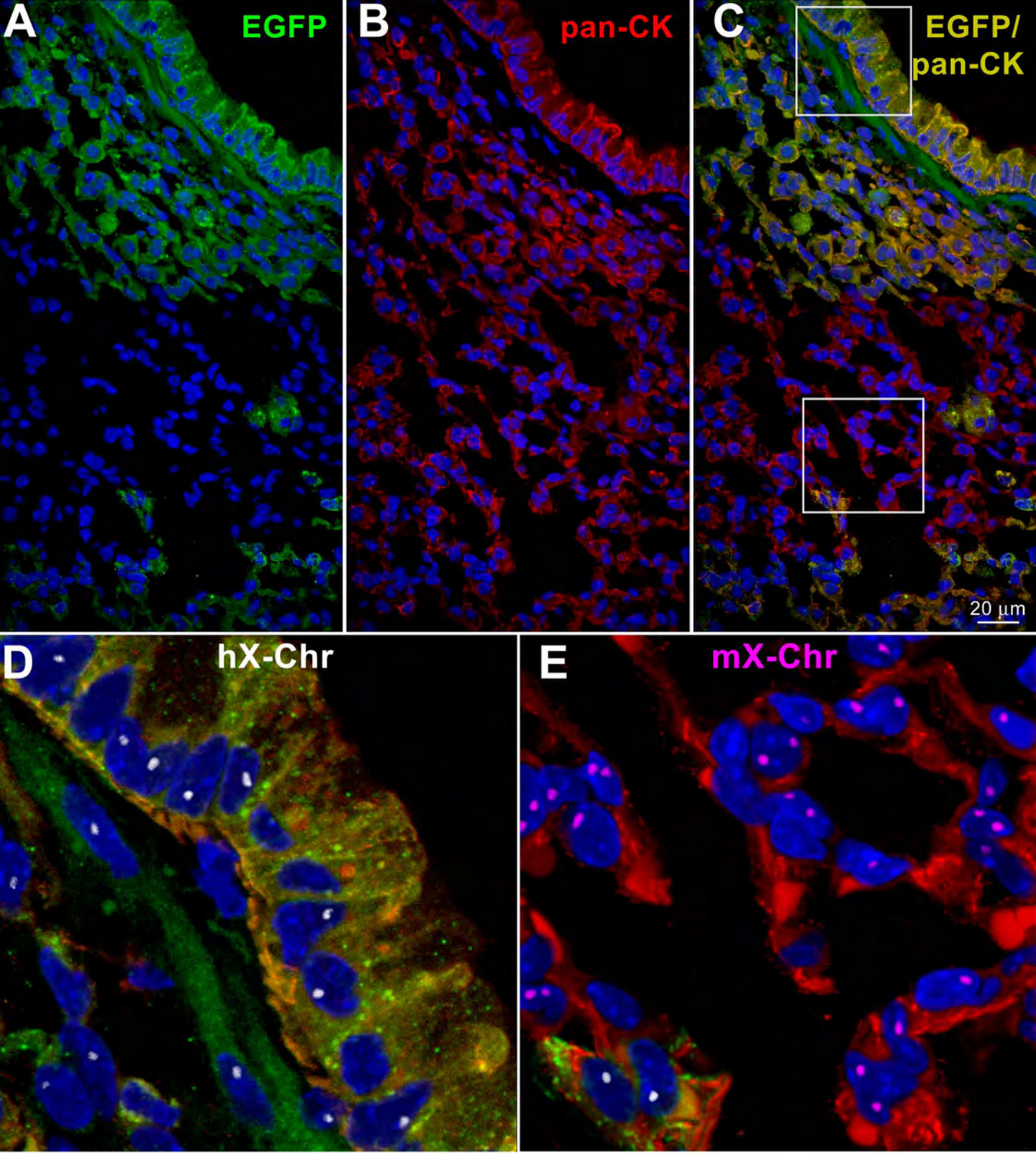

Supplementary Figure 17

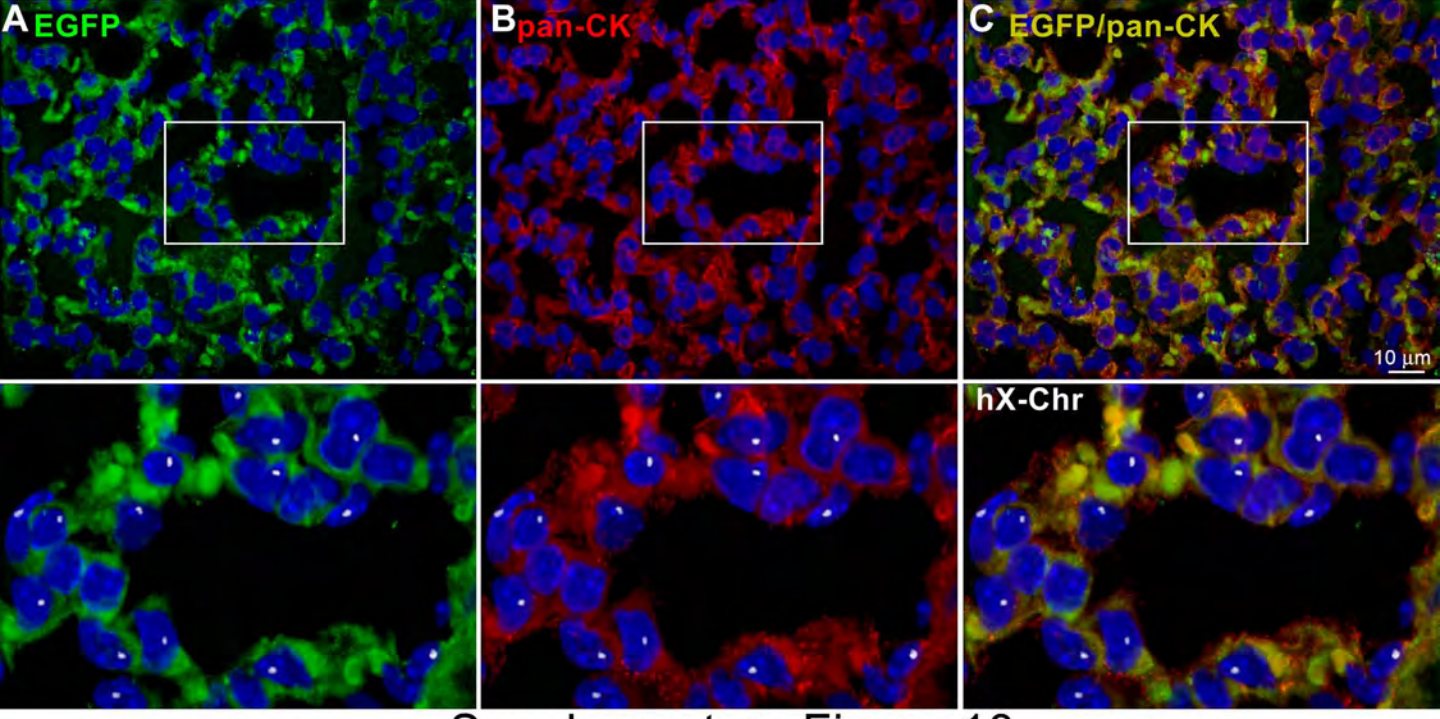

Supplementary Figure 18

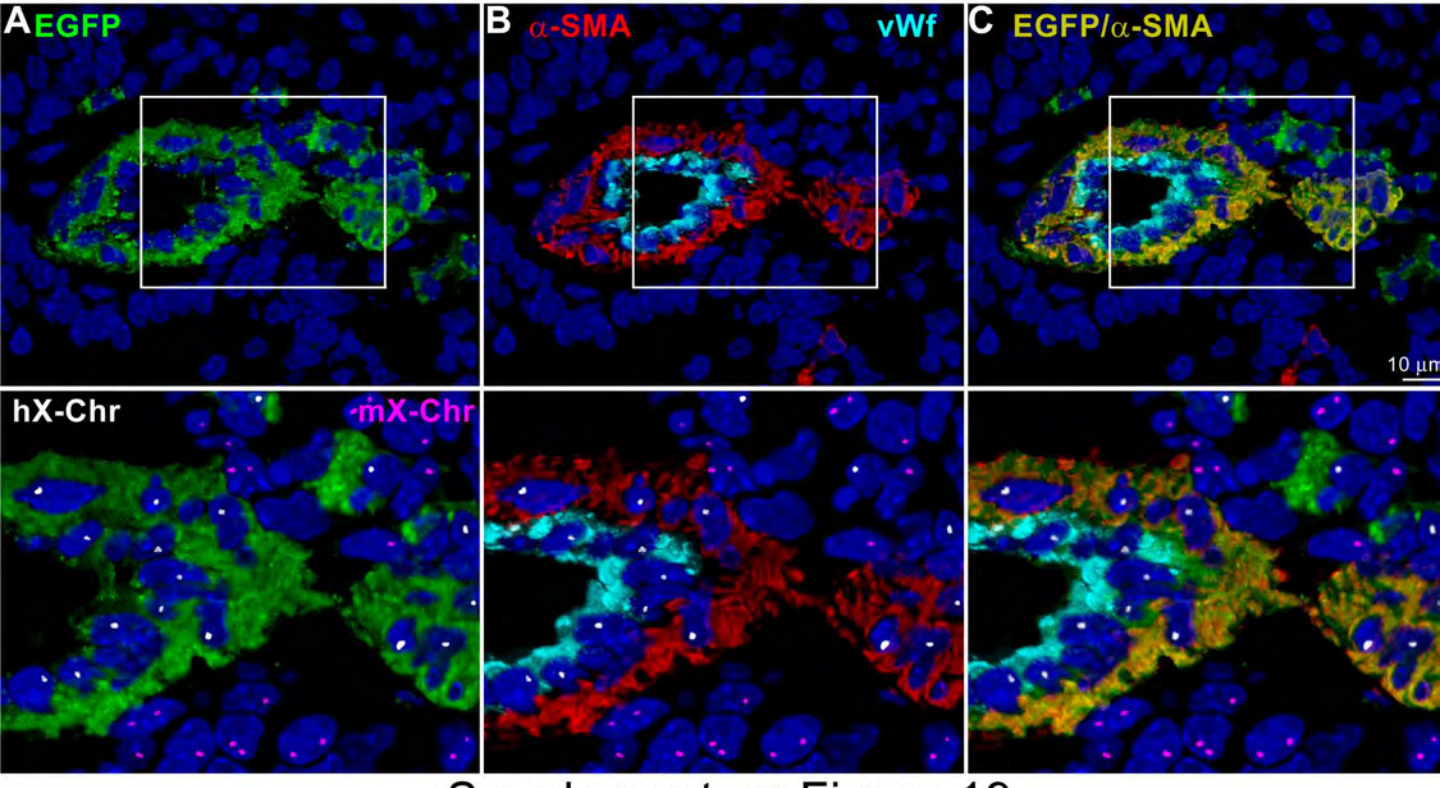

Supplementary Figure 19

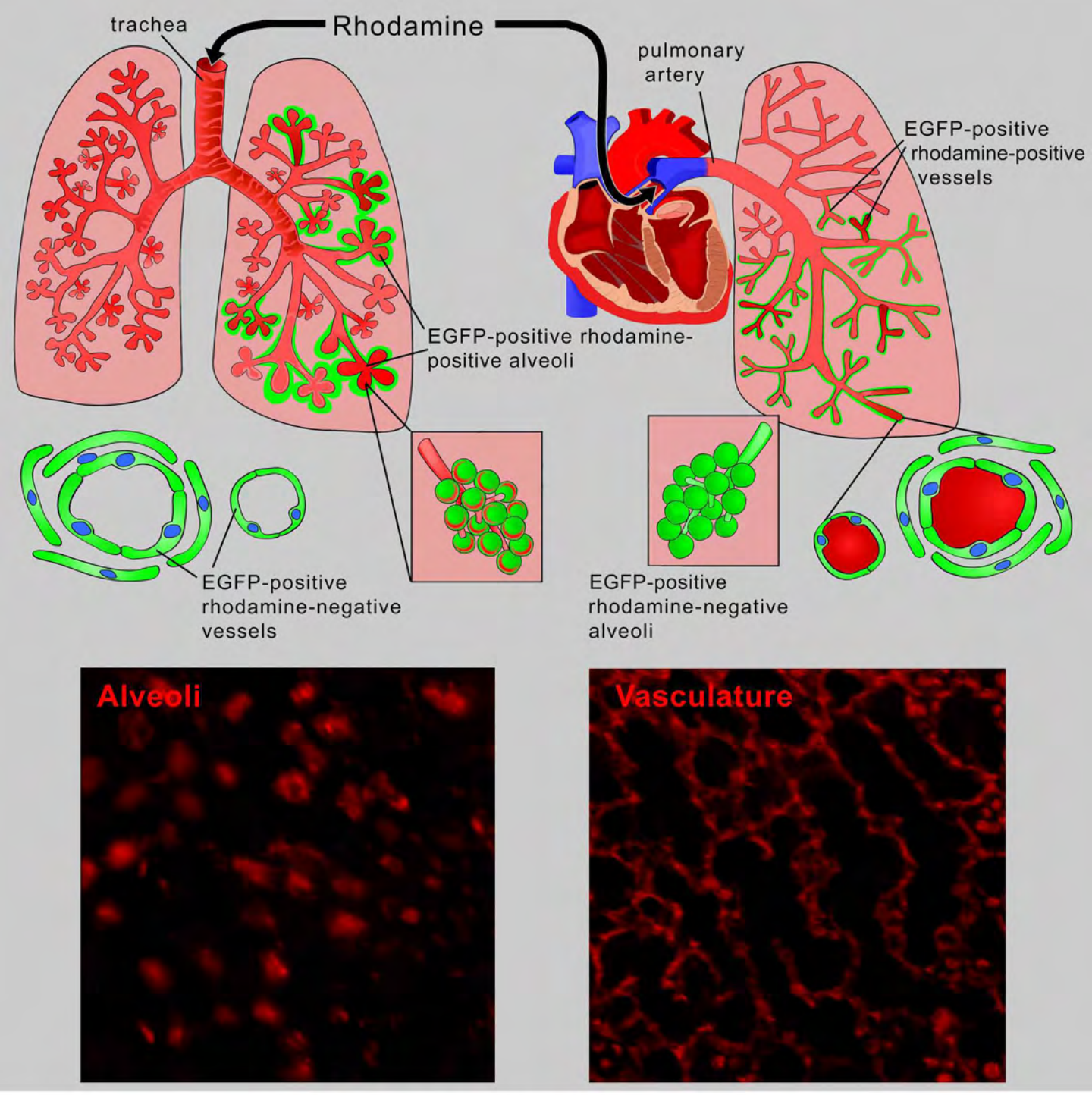

Supplementary Figure 20

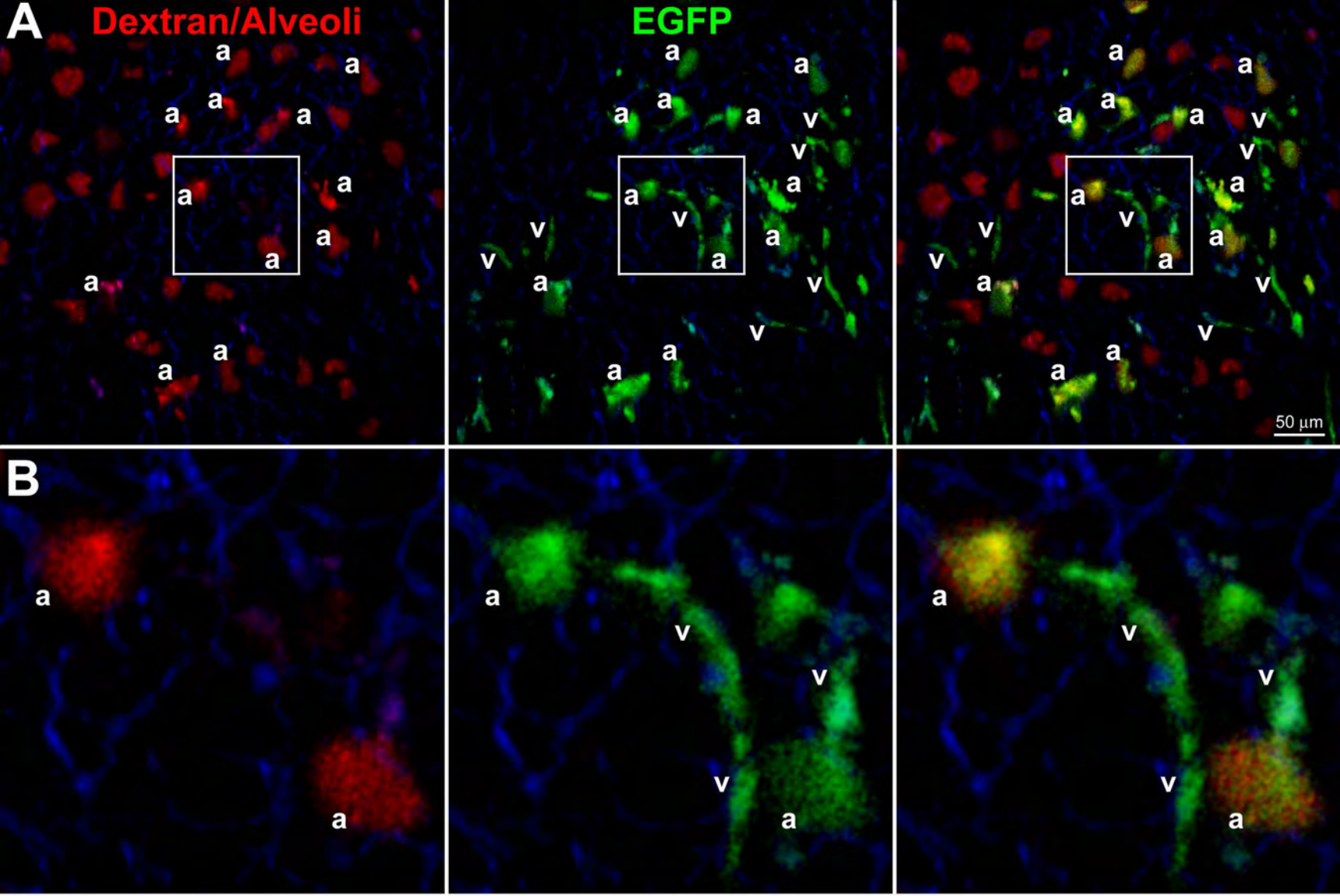

Supplementary Figure 21A, B

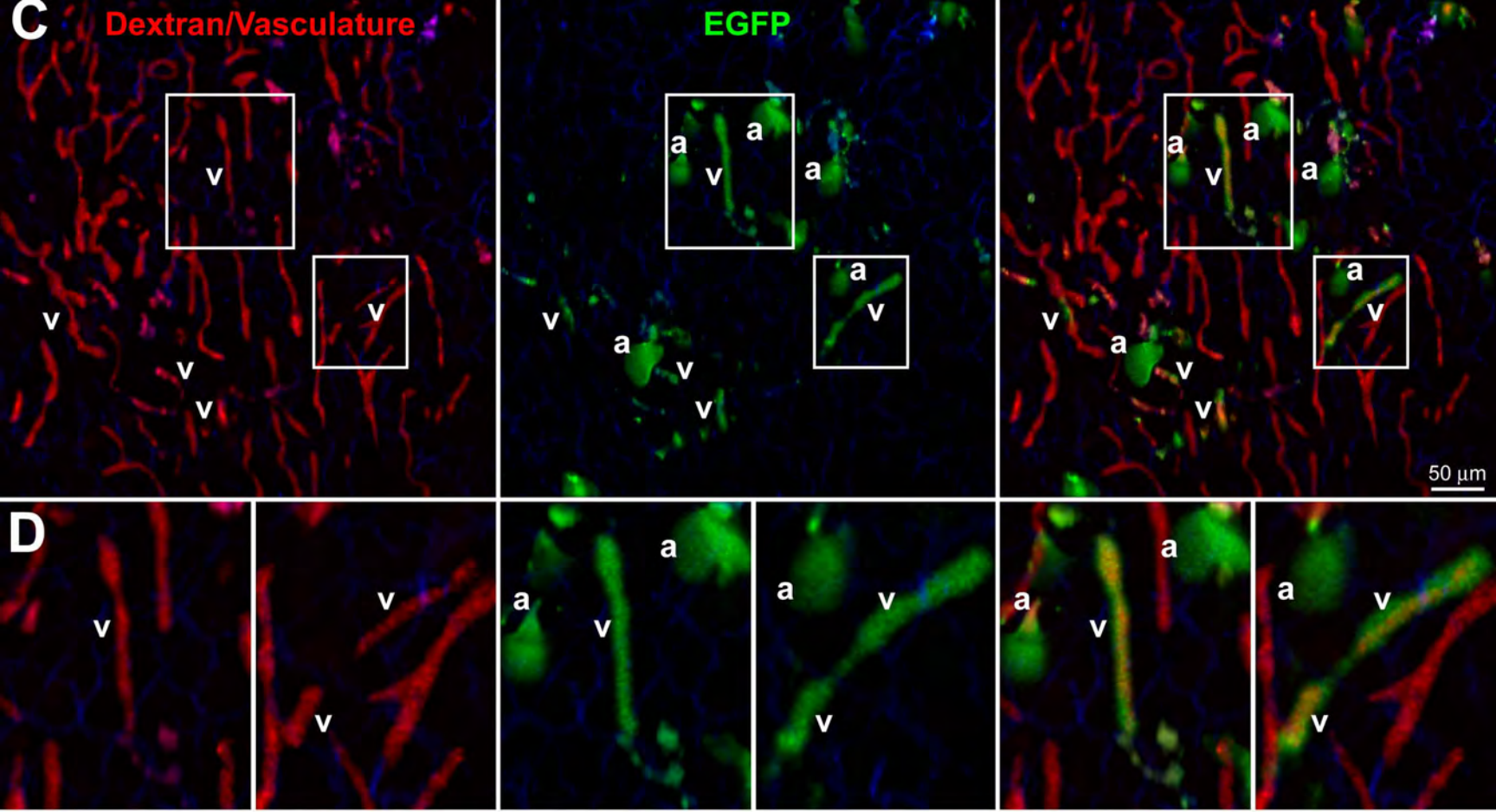

Supplementary Figure 21C, D

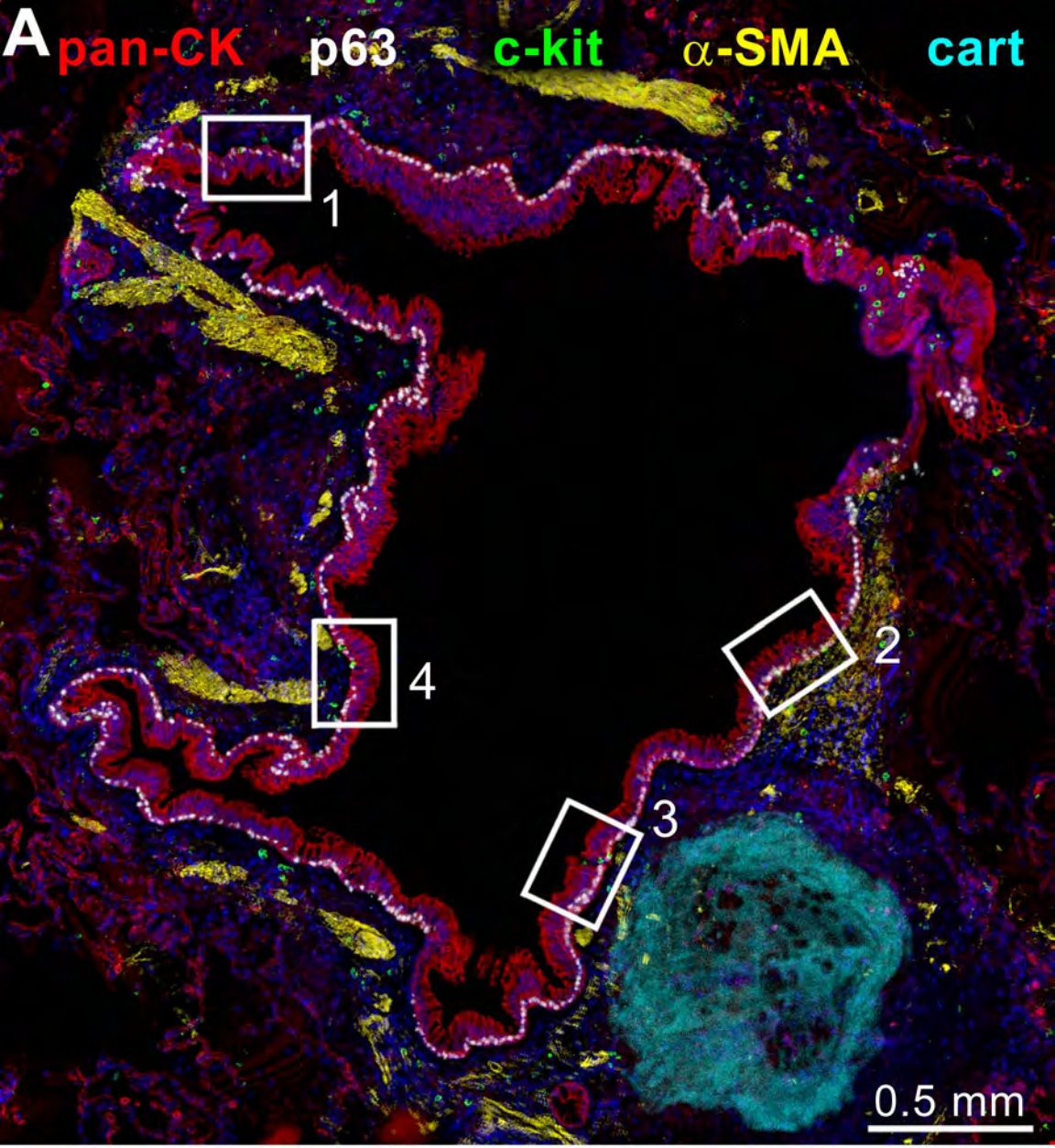

Supplementary Figure 22A, part 1

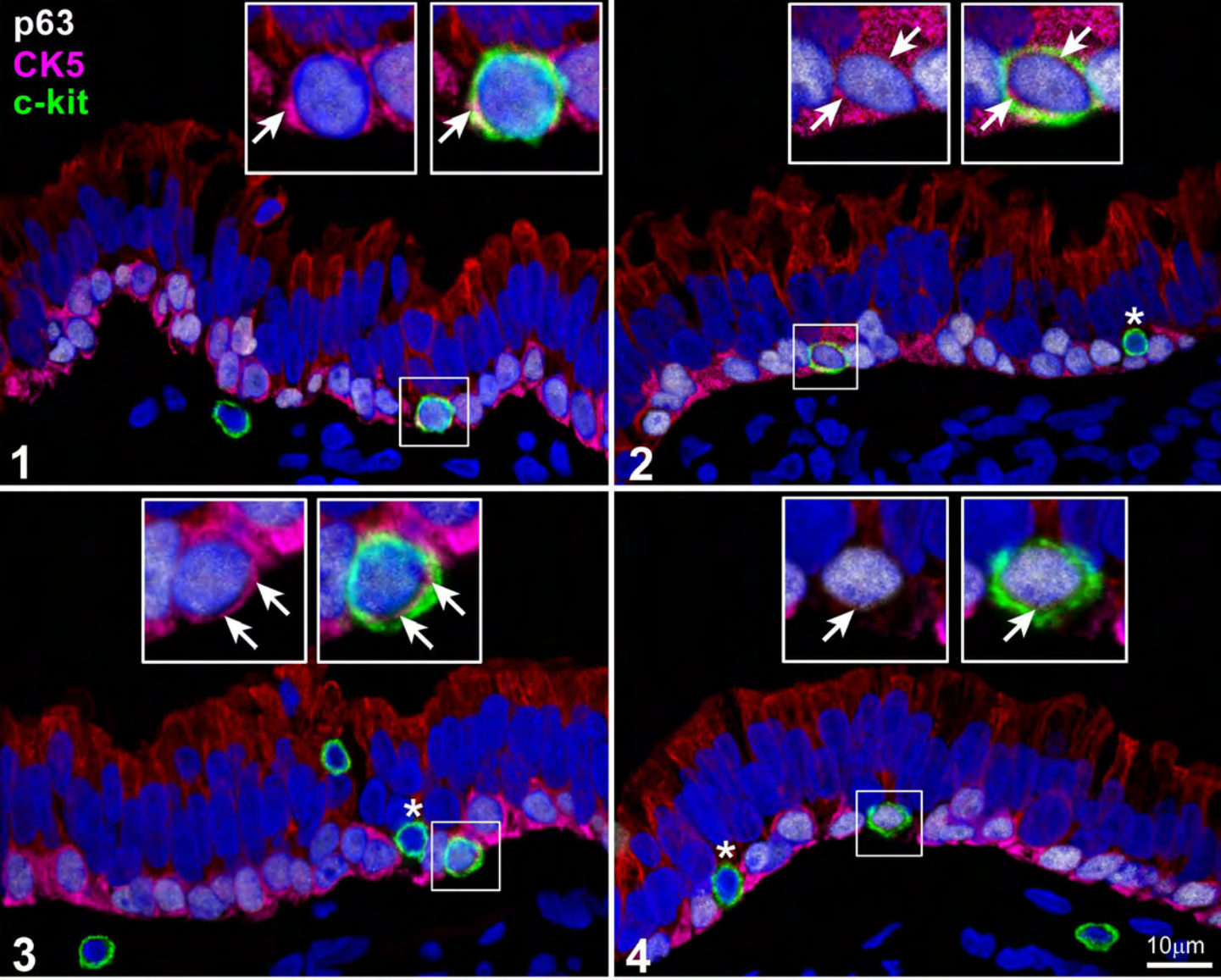

Supplementary Figure 22A, part 2

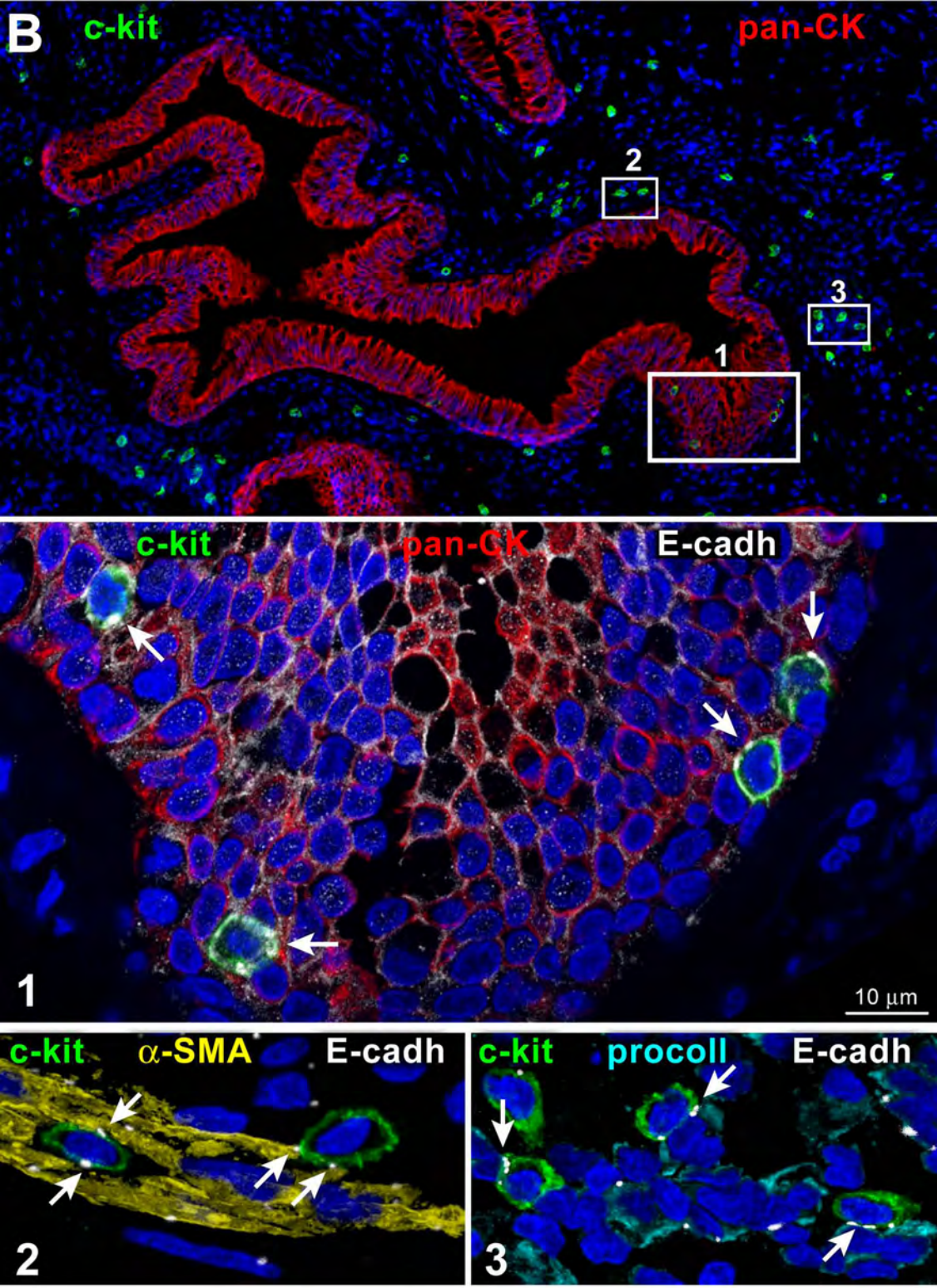

Supplementary Figure 22B

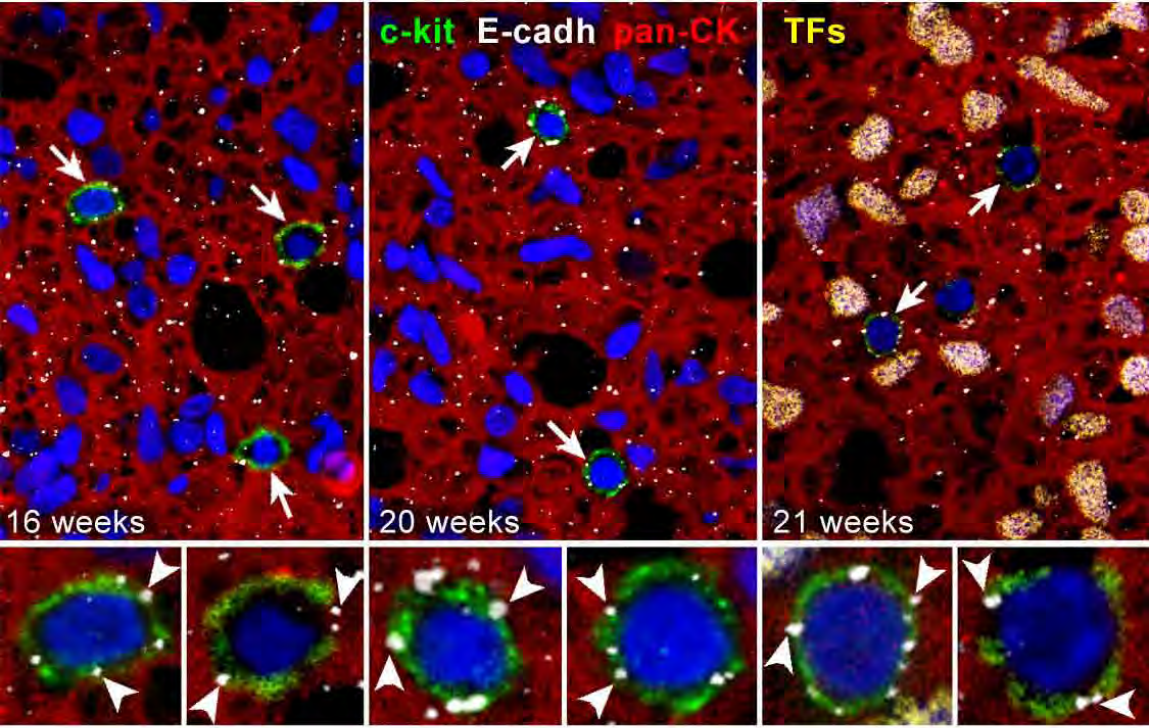

Supplementary Figure 23

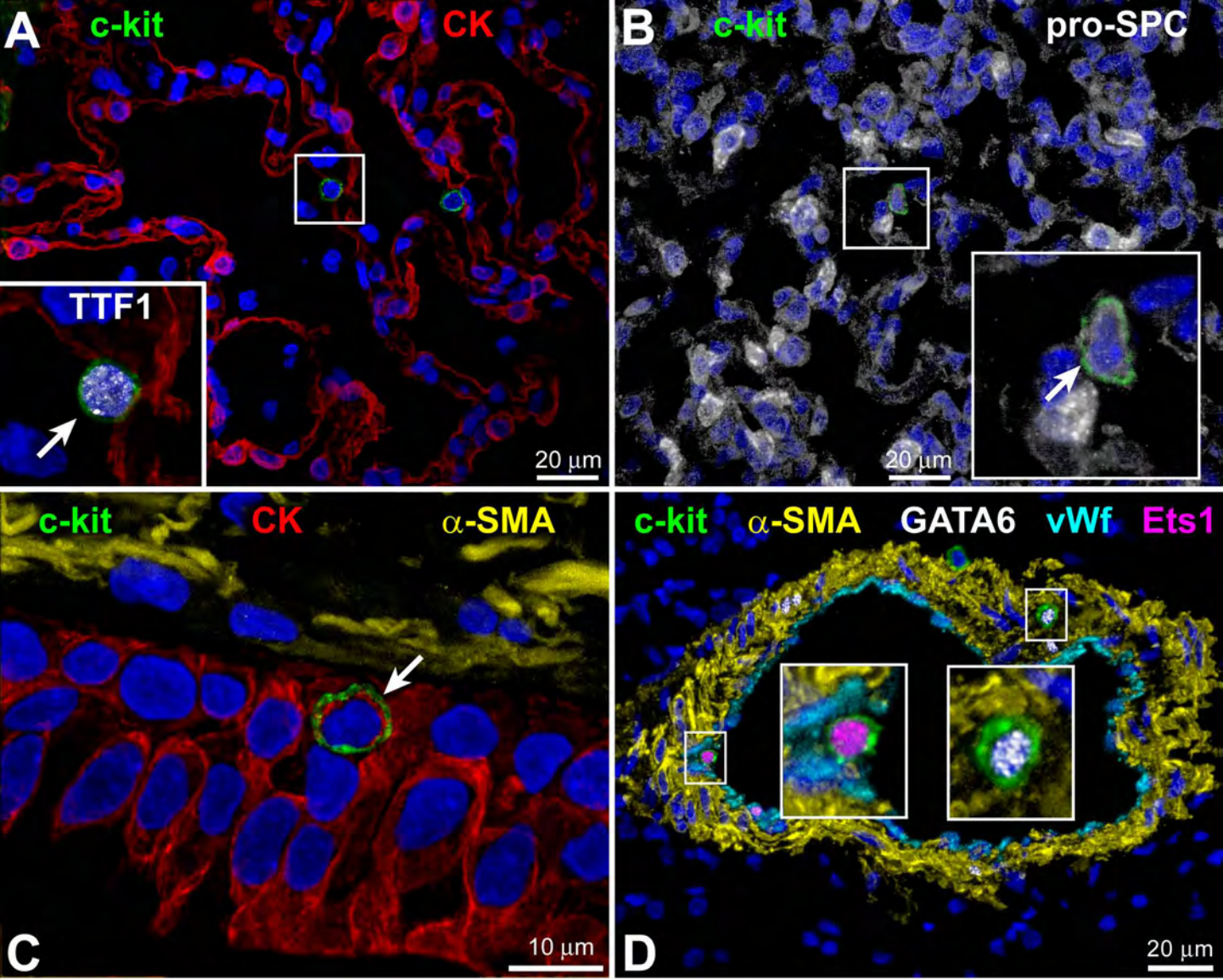

Supplementary Figure 24

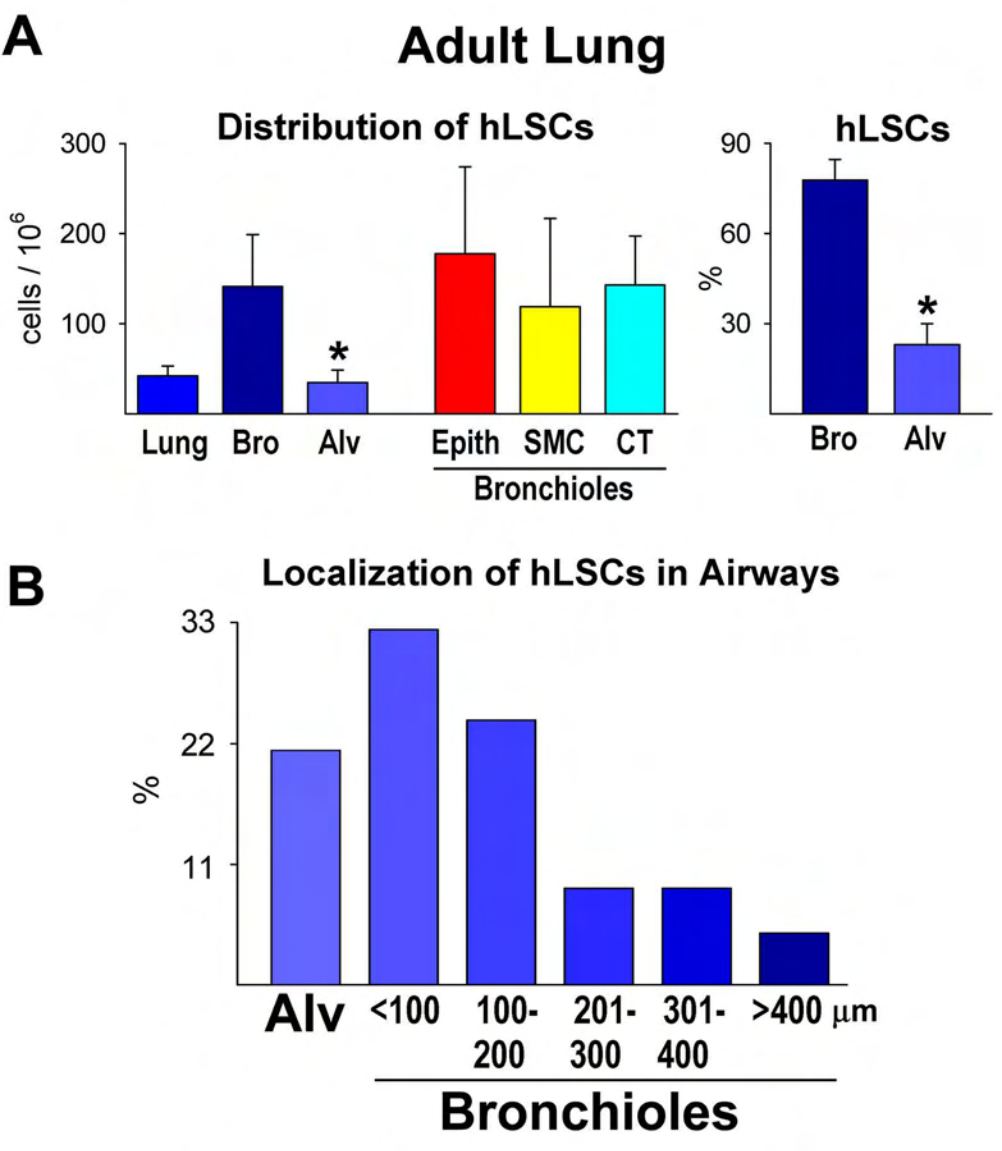

Supplementary Figure 25A, B

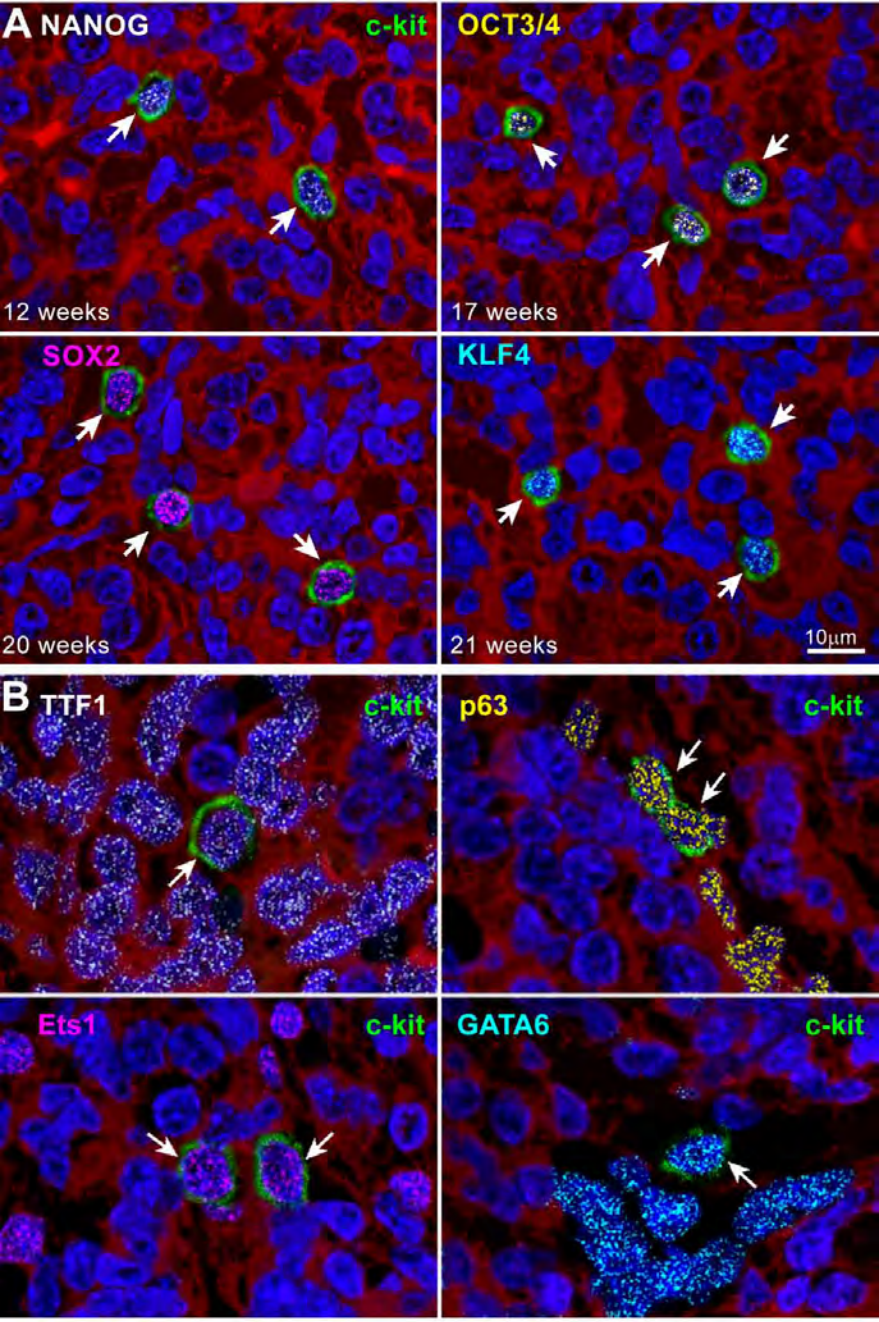

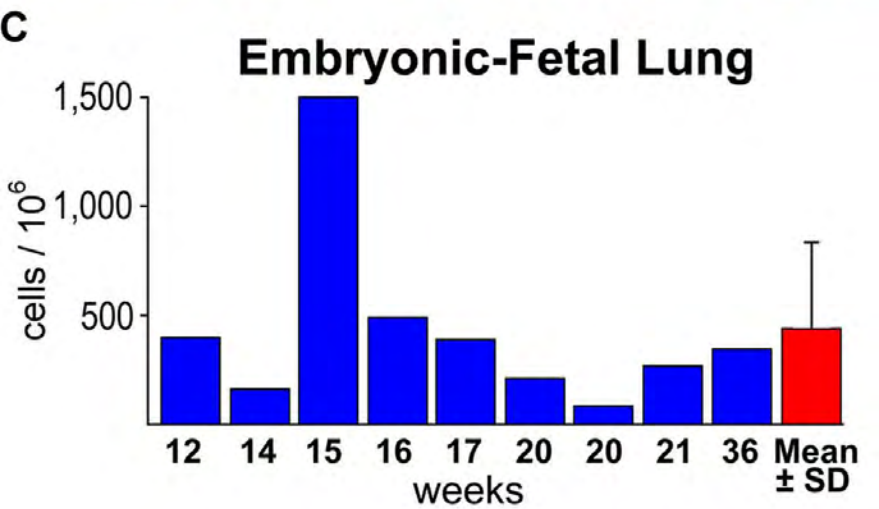

Supplementary Figure 26 A-C

METHODS

Human Lungs

The protocol employed to obtain discarded lung tissue was approved by the Partners Human Research Committee and the New England Organ Bank. Informed consent was obtained for research purposes of unused lung donor tissue samples. We studied 12 normal human lungs obtained from donor organs not employed for transplantation. Nine embryonic-fetal lungs were also studied. In the latter samples, the cause of death was acute trauma in one case, true knot of the umbilical cord in another instance, premature rupture of the chorioamniotic membrane in 2 cases, and voluntary pregnancy termination in 5 cases. Tissue sections from these embryonic-fetal lungs were obtained from the Department of Pathology, University of Parma Medical School, Parma, Italy.

Adult donor lungs were harvested by the transplant team and later declined for transplantation. Thus, the patients had 1) no known history of lung disease, 2) a chest x-ray without evidence of abnormalities, and 3) normal gas exchange (ratio of partial pressure of oxygen, PaO_2, to fractional concentration of oxygen, FiO_2, greater than 300). Moreover, all donors underwent bronchoscopy with bronchoalveolar lavage to assess lung injury or infection. These criteria excluded that the donor lungs had apparent pathologies. The majority of the harvested human lungs declined for transplantation were due to focal injury (focal aspiration in a single lung with the contralateral lung used for a transplant), anatomical variations of one of the lungs not allowing it to be transplanted, or lack of an appropriate recipient for one of the lungs with the contralateral lung being used

for transplant. During the harvesting procedure, the lungs were likely exposed to 100% oxygen for 1-2 hours while the donor was in the operating room. Additional information on the donor lungs, such as age, gender, and smoking history, was not available.

Lung samples were fixed in formalin and embedded in paraffin. These specimens were used to identify putative stem cell niches and putative human lung stem cells (hLSCs). The localization of these primitive cells in the distal airway was determined by immunolabeling with antibodies against the stem cell antigen c-kit.[1-4] Epithelial cells were labeled by TTF1, p63, pan-CK, CK-5, pro-SPC, SPC, CC10, and AQ-5; aggrecan was employed to label cartilage. ECs and vascular and non-vascular SMCs were detected with anti-vWf and anti-α-SMA, respectively. Fibroblasts were identified by procollagen. hLSCs were labeled with Oct3/4, Nanog, Sox2, and Klf4 antibodies. Adherens junctions between hLSCs and epithelial cells, SMCs, and fibroblasts were defined by the expression of E-cadherin (E-cadh). The presence of mast cells was assessed by the surface antigens CD6, CD29, CD45, CD49d, and CD49e, and the hydrolytic enzyme tryptase.[1-4] A complete list of antibodies and the modality of labeling for these epitopes are listed in Table 1 in the Supplementary Appendix.

Morphometric Analysis of hLSCs

Following the identification of hLSCs, the number of these primitive cells per mm^2 of alveolar parenchyma and bronchioles was determined, utilizing methodologies commonly employed in our laboratory.[5,6] Subsequently, the number of hLSCs per mm^2 of bronchiolar epithelial cells, SMCs, and peri-bronchiolar fibroblasts was evaluated. Similarly, the frequency of epithelial, SMC, and fibroblast nuclei in bronchioles and adjacent connective tissue was assessed. The diameter of hLSCs was next measured by

confocal microscopy; 20-30 hLSC profiles were sampled in each lung. From the distribution of hLSC diameters, the average hLSC volume and the number of hLSCs per cm^3 of lung tissue were obtained.[7,8] An identical protocol was employed for the quantitative analysis of hLSCs in the embryonic-fetal lung. As the specific gravity of the human lung[9] is $0.11 g/cm^3$, the number of hLSCs per unit mass was derived. The diameter of bronchioles was acquired by measuring the perimeter of each profile to compute the average diameter.

hLSCs

For the isolation of lung stem cells from fresh tissue, we obtained 8 samples from the Brigham and Women's Hospital Thoracic Surgery Tissue Bank. The tissue bank provides fresh tissue to investigators with IRB approval (protocol number 2008P000241). The lung tissue is obtained from patients sent to surgery for diagnosis of an abnormal focal lung process. The most normal appearing lung tissue from the periphery of the sample was provided for the harvest of cells. In two cases, the preserved structure was confirmed by histology and the absence of malignant-appearing cells documented.

The size of the specimens varied from 1-2 cm^3. For the isolation of hLSCs, fragments were enzymatically dissociated employing a protocol developed in our laboratory. By this methodology, tissue fragments were enzymatically dissociated in a solution containing collagenase to obtain a single cell suspension. Cells were expanded and, after FACS sorting, cell phenotype was defined by immunocytochemistry.[1-4] Putative hLSCs were then cultured in F12 medium (Gibco) supplemented with 10% FBS (Gibco).[3,4] At P2-P3, cells were characterized by FACS and immunolabeling to detect lineage negative hLSCs.[3,4]

FACS Analysis

This protocol included c-kit-positive hLSCs, c-kit negative lung cells, and CD34-positive human bone marrow cells (Lonza Inc.). C-kit-negative lung cells reflected the fraction of cells not recognized by immunomagnetic beads conjugated with the c-kit antibody. Additionally, CD34-positive human bone marrow cells were exposed to collagenase, 1 mg/ml, for 20 min at 37°C, to determine whether enzymatic digestion removed the specific surface epitopes. In all cases, cells were fixed in 4% paraformaldehyde for 15 min at room temperature and analyzed by FACS. C-kit-negative lung cells and CD34-positive human bone marrow cells treated by collagenase were tested for c-kit expression and for specific hematopoietic markers, respectively. C-kit-positive cells were tested for markers of hematopoietic cell lineages, mesenchymal stromal cells, mast cells, and transcription factors and cytoplasmic proteins typical of pulmonary cell classes. The antibodies used in this assay are listed in Table 1 in the Supplementary Appendix. This analysis was performed by FACSAria (Becton Dickinson). Cellular debris and aggregates were gated out based on forward scatter and side scatter. Gating on the signal of the nuclear stain DAPI was employed to exclude additional artifacts. Isotype-matched negative controls were utilized to define the threshold for each specific signal and establish the appropriate gate for positive cells.[1-4,10] Data were analyzed with the instrument software.

Immunocytochemistry of Isolated hLSCs

For immunolabeling, hLSCs were fixed in 4% paraformaldehyde for 15 min at room temperature. When possible, primary antibodies were directly labeled with fluorochromes (Molecular Probes) to avoid cross-reactivity.[3,4,11,12] Antibodies for immunocytochemistry

are listed in Table 1 in the Supplementary Appendix. Omission of the primary antibody and isotype-matched irrelevant antibodies were employed as negative controls. C-kit-negative lung cells (see above) were utilized to document the specificity of c-kit staining.

Cloning Assay and Clonal Cell Differentiation

FACS-sorted lineage-negative c-kit-positive cells were deposited in single wells of Terasaki plates or plated at limiting dilution, 1 cell/20 mm^2. In each culture dish, doublets of cells were excluded by microscopic examination. After 3-4 weeks, clones of identical cells were obtained.[1-4] Clones were collected directly from the Terasaki plates or by cloning cylinders and expanded in F12 medium.[3,4] Differentiation of clonal cells was induced by MEM containing 10% FBS and 10^{-8} M dexamethasone.[1-4] Cell phenotypes were defined by FACS analysis, qRT-PCR, Western blotting and immunocytochemistry. The inability of hLSCs to give rise to cardiac cell lineages and human cardiac stem cells to differentiate into pulmonary cells was established by FACS.

hLSC Division

Symmetric and asymmetric division[3,4,8] of hLSCs was determined by immunolabeling mitotic cells with α-adaptin antibody. Mitotic chromosomes were identified by staining with propidium iodide. To establish the fate of daughter cells, antibodies for markers of commitment to epithelial, endothelial and smooth muscle cells were employed: they included TTF1, Ets1, and GATA6, respectively.

Lentiviral Infection

hLSCs were infected with a lentivirus carrying EGFP in the presence of 8 μg/ml polybrene.[3,4,10] After overnight incubation at 37°C, fresh medium was added. Five days

later, the efficiency of infection was established by measuring the fraction of hLSCs showing native EGFP fluorescence. Efficiency of infection was 80±5 (n=7).

Lung Injury and Regeneration

Under ketamine (120 mg/kg bw) and xylazine (0.5 mg/kg bw) anesthesia,[3,11,12] C57Bl/6 female mice immunosuppressed with cyclosporine A (5 mg/kg/day) were mechanically ventilated, the chest opened, and a cryoinjury, ~2-3 mm^3 in volume, was induced in the left lung with a stainless steel probe pre-cooled in liquid nitrogen. The area of damage was identified by the pale color of the affected tissue. Shortly thereafter, 6 needle injections of clonal or non-clonal hLSCs, previously infected with a lentivirus carrying EGFP,[3,4,10,13] were administered in the region adjacent to the damaged parenchyma. Each injection consisted of ~20,000 cells mixed with 1% rhodamine-labeled polystyrene microspheres. This protocol allowed the direct visualization of the site of injection and the accuracy of cell delivery.[3,4,12,13] . In separate groups of animals, similar injections of human HSCs, hCSCs, and c-kit-negative human lung cells were performed. The chest was closed and the animals were allowed to recover. Injured mice not injected with hLSCs were used as controls. BrdU, 50 mg/kg body weight, was delivered i.p. twice a day to define the response of the mouse lung after injury. Animals were sacrificed at 12 hours, and 2 and 10-14 days following surgery by i.p. administration of sodium pentobarbital, 75 mg/kg bw. The lung was perfused through the trachea with PBS for 1 minute and with 10% phosphate-buffered formalin for 15 min.[14] Perfusion pressure was kept at 20 mmHg. Subsequently, the lung was excised, immersed in formalin for 24 hours, and embedded in paraffin.

Serial Transplantation of hLSCs

Ten-fourteen days after cryoinjury and hLSC implantation, regenerated lungs were excised and subjected to enzymatic digestion to obtain a single cell suspension. EGFP-positive c-kit-positive hLSCs were sorted by FACS and injected immediately in new recipient immunosuppressed mice following a protocol identical to that described above. Animals were sacrificed ten days later; the lung was excised, immersed in formalin for 24 hours, and embedded in paraffin.

Immunohistochemistry and In Situ Hybridization

Antibodies were used to detect human pulmonary structures within the recipient mouse lung (Table 1 in the Supplementary Appendix). Human cells were detected by EGFP localization and by in situ hybridization with a probe against the human-specific Alu repeat sequences.[3,4] Human X-chromosome and mouse X-chromosome were also identified.[3,4] Images were assembled with Adobe Photoshop 7.0 software according to the standard protocol detailed in the Nature guidelines for digital images. Processing included the assignment of pseudo-colors and changes in brightness. It was applied uniformly across the entire image and was used exclusively to equalize the appearance of multiple panels in a single figure.

Spectral Analysis

This methodology was performed with a Zeiss LSM510 Meta confocal microscope (Zeiss) utilizing the meta detector and the lambda acquisition mode. Lung sections were stained with DAPI only and the native fluorescence of EGFP was examined. Formalin-fixed tissue exhibits some autofluorescence due to cross-linking of proteins by the aldehyde groups of the fixative. The spectral properties of EGFP and formalin cross-linked cellular proteins are different. Intrinsic EGFP fluorescence was excited at 488 nm

with an argon laser and its fluorescence intensity was recorded generating a lambda stack ranging from 492 to 748 nm at 10.7 nm intervals. The lens and corresponding numerical aperture were 60X and 1.4, respectively.

For each region of interest, a graph plotting mean pixel intensity and the emission wavelength of the lambda stack was generated. To compare the shape of each curve obtained from EGFP-positive and EGFP-negative structures, the values of emission spectra were normalized by dividing the intensity of each wavelength by the peak signal. The spectrum obtained from EGFP-positive cells exhibited a major peak at ~525 nm, with a smaller peak at ~560 nm. In contrast, the spectrum of autofluorescence was more uniformly spread across the range of wavelengths and did not show a clearly defined peak of emission.[10,15-17] In an identical manner, we analyzed immunolabeled EGFP-positive structures, including epithelial cells and SMCs.

Two-Photon Microscopy

Ten-fourteen days after lung cryoinjury and implantation of EGFP-positive clonal or non-clonal hLSCs, the lungs together with the trachea and the heart were excised. Normal mouse lungs were employed to define the pattern of rhodamine labeling of alveoli and pulmonary vessels (Fig. 20 in the Supplementary Appendix). The preparation was placed in a bath mounted on the stage of a two-photon microscope (Bio-Rad Radiance 2100MP). Subsequently, the lungs were continuously perfused at a pressure of 20 mmHg through the trachea or pulmonary artery with PBS containing rhodamine-labeled dextran, which has a MW of 70 kDa and red fluorescence. This molecule does not cross the endothelial or epithelial barrier, allowing the visualization of the pulmonary vasculature or the respiratory tree, respectively. Rhodamine is covalently bound to dextran and has inherent

red fluorescence so that these two distinct pulmonary compartments could be detected by two-photon microscopy. Mouse recipient pulmonary structures were by necessity EGFP-negative while the regenerated distal airways and vessels were EGFP-positive, constituting the progeny of the injected hLSCs (Fig. 20 in the Supplementary Appendix).

All experiments were performed at 37°C. The microscope was positioned to view the area of injury and the adjacent parenchyma. EGFP and rhodamine were excited at 900 nm with a mode-locked Ti:Sapphire femtosecond laser (Tsunami, Spectra-Physics) and the corresponding images were acquired at emission wavelengths of 525 and 600 nm, respectively.[13,18-21] Collagen was visualized by second harmonic generation, which is the product of two-photon excitation and periodic structure of collagen. Thus, the red fluorescence of rhodamine-labeled dextran, the green fluorescence of EGFP, and the blue fluorescence of collagen were detected directly in the injured lung.

When the trachea was perfused with rhodamine-labeled dextran, the newly-formed airway structures were both EGFP-positive (green) and rhodamine-positive (red); however, with this approach, the regenerated pulmonary vasculature was EGFP-positive (green) and rhodamine-negative (non-red). Conversely, when the pulmonary artery was perfused with rhodamine-labeled dextran, the newly-formed vessels were both EGFP-positive (green) and rhodamine-positive (red) while the regenerated airways were EGFP-positive (green) and rhodamine-negative (non-red).

Quantitative RT-PCR

Total RNA was extracted with TRIzol from clonal hLSCs for the detection of transcripts for c-kit, the stemness genes Oct3/4, Nanog, Sox2 and Klf4, and epithelial lineage genes. CD34 human bone marrow cells and Kazumi lymphoma cells were used as positive

controls for c-kit expression. Additionally, RNA was obtained from the mouse lung 1-2 weeks after cryoinjury and injection of clonal and non-clonal hLSCs. cDNA was generated from 2 μg of total RNA incubated with oligo$(dT)_{15}$ primer for 2 hours at 37°C. RT-PCR was performed on 7300 Real Time PCR Systems (Applied Biosystems) using 1/20th of the cDNA per reaction.[21-23] Cycling conditions were as follows: 95°C for 10 minutes followed by 35 cycles of amplification (95°C denaturation for 15 seconds, and 60°C combined annealing/extension for 1 minute). Human-specific primers (see below) were designed with the Vector NTI software (Invitrogen). Quantified values were normalized against the input determined by the housekeeping human gene β2 microglobulin. Human lung total RNA (Applied Biosystems) and RNA extracted from an untreated mouse lung were used as positive and negative controls, respectively.

PCR products were run on 2% agarose/1x TBE gel and DNA bands with the expected molecular size were obtained. DNA was extracted with QIAquick Gel Extraction Kit (Qiagen), eluted in 30 μl of 10 mM Tris buffer (pH 8.5) and amplified by Platinum Blue PCR Supermix in the presence of the same forward and reverse primers used for real-time RT-PCR. PCR reaction was carried out in an Eppendorf Mastercycler.[21-23] Cycling conditions were as follows: 94°C for 2 minutes, followed by 20 cycles of amplification (94°C denaturation for 15 seconds, 60°C annealing for 30 seconds, 72°C elongation for 15 seconds) with a final incubation at 72°C for 2 minutes. After purification using QIAquick PCR Purification kit, samples were submitted to the DNA Sequencing Facility at Dana-Farber/Harvard Cancer Center to obtain the DNA sequence. The human origin of the transcripts was confirmed by employing BLAST searches.

Mouse ACTB (β-actin; amplicon size: 126 bp) [cross-react with Human]

Forward: 5'- AGAAGGAGATTACTGCTCTGGCTC -3'

Reverse: 5'- ACATCTGCTGGAAGGTGGACA -3'

B2M (β2 microglobulin; amplicon size: 176 bp)

Forward: 5'- CAAGGACTGGTCTTTCTATCTCTTG -3'

Reverse: 5'- ATTCATCCAATCCAAATGCG -3'

c-kit (amplicon size:146 bp)

Forward: 5'- GCACCTGCTGAAATGTATGACATAAT -3'

Reverse: 5'- CTGCAGTTTGCTAAGTTGGAGTAAAT -3'

OCT3/4 (amplicon size: 165 bp)

Forward: 5'- AGGAGAAGCTGGAGCAAAA - 3'

Reverse: 5' - GGCTGAATACCTTCCCAAA - 3'

NANOG (amplicon size: 133 bp)

Forward: 5'- GGTCCCGGTCAAGAAACAGA - 3'

Reverse: 5' - GAGGTTCAGGATGTTGGAGA - 3'

SOX2 (amplicon size: 155 bp)

F: CCAGCTCGCAGACCTACA

R: CCTGGAGTGGGAGGAAGA

KLF4 (amplicon size: 144 bp)

Forward: 5' - GACTTCCCCCAGTGCTTC - 3'

Reverse: 5' - CGTTGAACTCCTCGGTCTC - 3'

TP63 (amplicon size: 185 bp)

Forward: 5'- AAAGCAGCAAGTTTCGGACAGTAC - 3'

Reverse: 5’ - CCAGGGACTCTTTGATCTTCAACAG - 3’

KRT5 (cytokeratin 5; amplicon size: 162 bp)

Forward: 5’- AGGGCGAGGAATGCAGACTC - 3’

Reverse: 5’ - TGCTACCTCCGGCAAGACCT - 3’

TTF1 (Nkx2-1; amplicon size: 116 bp)

Forward: 5’- CATGAGGAACAGCGCCTCTG -3’

Reverse: 5’- CGCCCATGCCGCTCATG -3’

SCGB1A1 (Clara cells 10 kDa secretory protein; amplicon size: 191 bp)

Forward: 5’- TCACCCTCACCCTGGTCACA -3’

Reverse: 5’- GGTGTCCACCAGCTTCTTCAGC -3’

SFTPC (surfactant protein C; amplicon size: 161 bp)

Forward: 5’- CACTGGCCTCGTGGTGTATG -3’

Reverse: 5’- CCTGCAGAGAGCATTCCATC -3’

CFTR (cystic fibrosis transmembrane conductance regulator; amplicon size: 159 bp)

Forward: 5’- GAAGCAATGCTGGAATGCCAAC -3’

Reverse: 5’- CTTGCTTGAGTTCCGGTGGG -3’

KRT18 (keratin 18; amplicon size: 164 bp)

Forward: 5’- CTGGAAGATGGCGAGGACTTTAATC -3’

Reverse: 5’- GGTACCCTGCTTCTGCTGG -3’

T1α (podoplanin; amplicon size: 175 bp)

Forward: 5’- CAGTCCACGCGCAAGAACAAAG -3’

Reverse: 5’- GCACCAATGAAGCCGATGGC -3’

AQP5 (aquaporin 5; amplicon size: 198 bp)

Forward: 5'- GTCCATTGGCCTGTCTGTCACC -3'

Reverse: 5'- GAGTTGGGGAAGAGCAGGTAGAAG -3'

ETS1 (v-ets erythroblastosis virus E26 oncogene homolog 1; amplicon size: 186 bp)

Forward: 5'- GCTATCAAACAAGAAGTCGTCACC -3'

Reverse: 5'- GAAGCTGTCATAGGAGGGAACA -3'

PECAM1 (CD31; amplicon size: 194 bp)

Forward: 5'- TAAAGAGCCTCTGAACTCAGACG -3'

Reverse: 5'- CATCTGGCCTTGCTGTCTAAG -3'

TGFBR1 (TGF β receptor 1; amplicon size: 191 bp)

Forward: 5'- CAAACCACAGAGTGGGAACA -3'

Reverse: 5'- TACAAGATCATAATAAGGCAGTTGG -3'

Immunoprecipitation and Western Blotting

Protein lysates of hLSCs before and after exposure to dexamethasone were obtained using RIPA buffer (Sigma) and protease inhibitors. Equivalents of 20-50 μg of proteins were separated on 8-12% SDS-PAGE, transferred onto PVDF membranes (Bio-Rad) and subjected to Western blotting with Oct3/4 (rabbit polyclonal, Novus Biologicals), Nanog (rabbit polyclonal, Abnova), Sox2 (mouse monoclonal, Abcam), and Klf4 (mouse monoclonal, Abcam) antibodies diluted 1:100 in TBST overnight at 4ºC. HRP-conjugated anti-IgG were used as secondary antibodies. Proteins were detected by chemiluminescence (SuperSignal West Femto Maximum Sensitivity Substrate, Thermo Scientific) and optical density was measured. Loading conditions were determined by the expression of GAPDH (Millipore) and/or by Ponceau S (Sigma) staining of the membrane after transfer.[19,22,23] For c-kit expression, 50-100 μg of proteins were

immunoprecipitated with c-kit antibody (mouse monoclonal, Serotec) and subjected to Western blotting with c-kit antibody (rabbit polyclonal, Cell Signaling; #3074). CD34-positive bone marrow cells and Kazumi lymphoma cells were used as positive controls. The mature form of the c-kit receptor, capable of binding stem cell factor, corresponds to a 145 kDa band. The lower molecular weight form of c-kit at 120 kDa was also found.

Statistical Analysis

The number of animals in each study and the magnitude of sampling employed in each in vitro and in vivo determination are listed in Table 2 in the Supplementary Appendix. In all cases, results are presented as mean±SD. Statistical significance was determined by the analysis of variance and Bonferroni method or Student's t test; $P<0.05$ was considered significant.[24]

References

1. Beltrami AP, Barlucchi L, Torella D, Baker M, Limana F, Chimenti S, Kasahara H, Rota M, Musso E, Urbanek K, Leri A, Kajstura J, Nadal-Ginard B, Anversa P. Adult cardiac stem cells are multipotent and support myocardial regeneration. Cell 2003;114:763-76.

2. Linke A, Müller P, Nurzynska D, Casarsa C, Torella D, Nascimbene A, Castaldo C, Cascapera S, Böhm M, Quaini F, Urbanek K, Leri A, Hintze TH, Kajstura J, Anversa P. Stem cells in the dog heart are self-renewing, clonogenic, and multipotent and regenerate infarcted myocardium, improving cardiac function. Proc Natl Acad Sci USA 2005;102:8966-71.

3. Bearzi C, Rota M, Hosoda T, Tillmanns J, Nascimbene A, De Angelis A, Yasuzawa-Amano S, Trofimova I, Siggins RW, LeCapitaine N, Cascapera S, Beltrami AP,

D'Alessandro DA, Zias E, Quaini F, Urbanek K, Michler RE, Bolli R, Kajstura J, Leri A, Anversa P. Human cardiac stem cells. Proc Natl Acad Sci USA 2007;104:14068-73.

4. Bearzi C, Leri A, Lo Monaco F, Rota M, Gonzalez A, Hosoda T, Pepe M, Qanud K, Ojaimi C, Bardelli S, D'Amario D, D'Alessandro DA, Michler RE, Dimmeler S, Zeiher AM, Urbanek K, Hintze TH, Kajstura J, Anversa P. Identification of a coronary vascular progenitor cell in the human heart. Proc Natl Acad Sci USA 2009;106:15885-90.

5. Loud AV, Anversa P. Morphometric analysis of biologic processes. Lab Invest 1984; 50:250-61.

6. Anversa P, Olivetti G (2002) in Handbook of Physiology, eds. Page E, Fozzard H, Solaro R. (Oxford University Press, New York) Section 2, Vol. 1, pp 75-144.

7. Urbanek K, Quaini F, Tasca G, Torella D, Castaldo C, Nadal-Ginard B, Leri A, Kajstura J, Quaini E, Anversa P. Intense myocyte formation from cardiac stem cells in human cardiac hypertrophy. Proc Natl Acad Sci USA 2003;100:10440-5.

8. Urbanek K, Torella D, Sheikh F, De Angelis A, Nurzynska D, Silvestri F, Beltrami CA, Bussani R, Beltrami AP, Quaini F, Bolli R, Leri A, Kajstura J, Anversa P. Myocardial regeneration by activation of multipotent cardiac stem cells in ischemic heart failure. Proc Natl Acad Sci USA 2005;12:8692-7.

9. Nelson MD, Haykowsky MJ, Mayne JR, Jones RL, Petersen SR. Effects of self-contained breathing apparatus on ventricular function during strenuous exercise. J Appl Physiol 2009;106:395-402.

10. Hosoda T, D'Amario D, Cabral-Da-Silva MC, Zheng H, Padin-Iruegas ME, Ogorek B, Ferreira-Martins J, Yasuzawa-Amano S, Amano K, Ide-Iwata N, Cheng W, Rota M,

Urbanek K, Kajstura J, Anversa P, Leri A. Clonality of mouse and human cardiomyogenesis in vivo. Proc Natl Acad Sci USA 2009;106:17169-74.

11. Urbanek K, Cesselli D, Rota M, Nascimbene A, De Angelis A, Hosoda T, Bearzi C, Boni A, Bolli R, Kajstura J, Anversa P, Leri A. Stem cell niches in the adult mouse heart. Proc Natl Acad Sci USA 2006;103:9226-31.

12. Rota M, Kajstura J, Hosoda T, Bearzi C, Vitale S, Esposito G, Iaffaldano G, Padin-Iruegas ME, Gonzalez A, Rizzi R, Small N, Muraski J, Alvarez R, Chen X, Urbanek K, Bolli R, Houser SR, Leri A, Sussman MA, Anversa P. Bone marrow cells adopt the cardiomyogenic fate in vivo. Proc Natl Acad Sci USA 2007;104:17783-8.

13. Tillmanns J, Rota M, Hosoda T, Misao Y, Esposito G, Gonzalez A, Vitale S, Parolin C, Yasuzawa-Amano S, Muraski J, De Angelis A, LeCapitaine N, Siggins RW, Loredo M, Bearzi C, Bolli R, Urbanek K, Leri A, Kajstura J, Anversa P. Formation of large coronary arteries by cardiac progenitor cells. Proc Natl Acad Sci USA 2008;105:1668-73.

14. Song Y, Coleman L, Shi J, Beppu H, Sato K, Walsh K, Loscalzo J, Zhang YY. Inflammation, endothelial injury, and persistent pulmonary hypertension in heterozygous BMPR2-mutant mice. Am J Physiol 2008;295:H677-90.

15. D'Alessandro DA, Kajstura J, Hosoda T, Gatti A, Bello R, Mosna F, Bardelli S, Zheng H, D'Amario D, Padin-Iruegas ME, Carvalho AB, Rota M, Zembala MO, Stern D, Rimoldi O, Urbanek K, Michler RE, Leri A, Anversa P. Progenitor cells from the explanted heart generate immunocompatible myocardium within the transplanted donor heart. Circ Res 2009;105:1128-40.

16. Kajstura J, Urbanek K, Perl S, Hosoda T, Zheng H, Ogórek B, Ferreira-Martins J, Goichberg P, Rondon-Clavo C, Sanada F, D'Amario D, Rota M, Del Monte F, Orlic D,

Tisdale J, Leri A, Anversa P. Cardiomyogenesis in the adult human heart. Circ Res 2010;107:305-15.

17. Kajstura J, Gurusamy N, Ogórek B, Goichberg P, Clavo-Rondon C, Hosoda T, D'Amario D, Bardelli S, Beltrami AP, Cesselli D, Bussani R, del Monte F, Quaini F, Rota M, Beltrami CA, Buchholz BA, Leri A, Anversa P. Myocyte turnover in the aging human heart. Circ Res In press, 2010.

18. Dawn B, Stein AB, Urbanek K, Rota M, Whang B, Rastaldo R, Torella D, Tang XL, Rezazadeh A, Kajstura J, Leri A, Hunt G, Varma J, Prabhu SD, Anversa P, Bolli R. Cardiac stem cells delivered intravascularly traverse the vessel barrier, regenerate infarcted myocardium, and improve cardiac function. Proc Natl Acad Sci USA 2005;102:3766-71.

19. Urbanek K, Rota M, Cascapera S, Bearzi C, Nascimbene A, De Angelis A, Hosoda T, Chimenti S, Baker M, Limana F, Nurzynska D, Torella D, Rotatori F, Rastaldo R, Musso E, Quaini F, Leri A, Kajstura J, Anversa P. Cardiac stem cells possess growth factor-receptor systems that after activation regenerate the infarcted myocardium, improving ventricular function and long-term survival. Circ Res 2005;97:663-73.

20. Rota M, Padin-Iruegas ME, Misao Y, De Angelis A, Maestroni S, Ferreira-Martins J, Fiumana E, Rastaldo R, Arcarese ML, Mitchell TS, Boni A, Bolli R, Urbanek K, Hosoda T, Anversa P, Leri A, Kajstura J. Local activation or implantation of cardiac progenitor cells rescues scarred infarcted myocardium improving cardiac function. Circ Res 2008;103:107-16.

21. Gonzalez A, Rota M, Nurzynska D, Misao Y, Tillmanns J, Ojaimi C, Padin-Iruegas ME, Müller P, Esposito G, Bearzi C, Vitale S, Dawn B, Sanganalmath SK, Baker M,

Hintze TH, Bolli R, Urbanek K, Hosoda T, Anversa P, Kajstura J, Leri A. Activation of cardiac progenitor cells reverses the failing heart senescent phenotype and prolongs lifespan. Circ Res 2008;102:597-606.

22. Boni A, Urbanek K, Nascimbene A, Hosoda T, Zheng H, Delucchi F, Amano K, Gonzalez A, Vitale S, Ojaimi C, Rizzi R, Bolli R, Yutzey KE, Rota M, Kajstura J, Anversa P, Leri A. Notch1 regulates the fate of cardiac progenitor cells. Proc Natl Acad Sci USA 2008;105:15529-34.

23. Urbanek K, Cabral-da-Silva MC, Ide-Iwata N, Maestroni S, Delucchi F, Zheng H, Ferreira-Martins J, Ogórek B, D'Amario D, Bauer M, Zerbini G, Rota M, Hosoda T, Liao R, Anversa P, Kajstura J, Leri A. Inhibition of notch1-dependent cardiomyogenesis leads to a dilated myopathy in the neonatal heart. Circ Res 2010;107:429-41.

24. Berenson ML, Levine DM, Rindskopf D (1988) in Applied Statistics (Prentice Hall, Englewood Cliffs) pp 362-418.

Table 1. Antibodies and Probes

Epitope	Manufacturer	Host Animal	Labeling
Cytoplasmic markers			
EGFP	Molecular Probes	rabbit polyclonal	direct indirect FITC, TRITC
Pan-cytokeratin	Sigma	mouse monoclonal	direct indirect TRITC, Cy5
Cytokeratin 5	Epitomics	rabbit monoclonal	indirect TRITC, Cy5
pro-SPC	Abcam	rabbit polyclonal	indirect FITC, TRITC, Cy5
SPC	Sigma	rabbit polyclonal	indirect TRITC, Cy5
*CC10	Abcam	rabbit polyclonal	indirect FITC, TRITC, Cy5
α-SMA	Sigma	mouse monoclonal	direct indirect TRITC, Cy5
vWf	DAKO	rabbit polyclonal	indirect TRITC, Cy5
Tryptase	Abcam	mouse monoclonal	indirect TRITC, Cy5
Procollagen	Santa Cruz	goat polyclonal	indirect TRITC, Cy5
Aggrecan	Santa Cruz	rabbit polyclonal	indirect Cy5

α-adaptin	Abcam	mouse monoclonal	indirect Cy5
Nuclear markers			
TTF1	Abcam	rabbit polyclonal	indirect FITC, TRITC
p63	Abcam	rabbit polyclonal	indirect FITC, Cy5
Ets1	Abcam	rabbit polyclonal	indirect FITC, TRITC
GATA6	Abcam	rabbit polyclonal	indirect FITC, TRITC
SOX2	Abcam	mouse monoclonal	indirect TRITC, Cy5
OCT3/4	Abcam	rabbit polyclonal	indirect TRITC, Cy5
KLF4	Abcam	rabbit polyclonal	indirect TRITC, Cy5
NANOG	Abcam	rabbit polyclonal	indirect TRITC, Cy5
Alu	Biogenex	N/A	direct, indirect Cy5
Human X-chromosome	Vysis	N/A	direct FITC
Mouse X-chromosome	Cambio	N/A	direct Cy3
BrdU	Roche	mouse monoclonal	indirect TRITC, Cy5
Membrane markers			
c-kit	DAKO	rabbit polyclonal	indirect FITC, TRITC, Cy5

E-cadherin	Sigma	rabbit polyclonal	direct indirect TRITC,
Aquaporin-5	Abcam	rabbit polyclonal	indirect TRITC, Cy5
CD6	Abcam	mouse monoclonal	indirect Cy5
CD29	Abcam	mouse monoclonal	indirect Cy5
CD34	Becton Dickinson	mouse monoclonal	direct, indirect Cy5
CD44	Becton Dickinson	mouse monoclonal	direct, indirect Cy5
CD45	Becton Dickinson	mouse monoclonal	direct, indirect Cy5
CD49d	Abcam	rat monoclonal	indirect Cy5
CD49e	Abcam	mouse monoclonal	indirect Cy5
CD90	Becton Dickinson	mouse monoclonal	direct, indirect Cy5
CD105	Becton Dickinson	mouse monoclonal	direct, indirect Cy5
CD133	Abcam	mouse monoclonal	indirect Cy5
Lineage markers	Becton Dickinson	mouse monoclonal	indirect Cy5

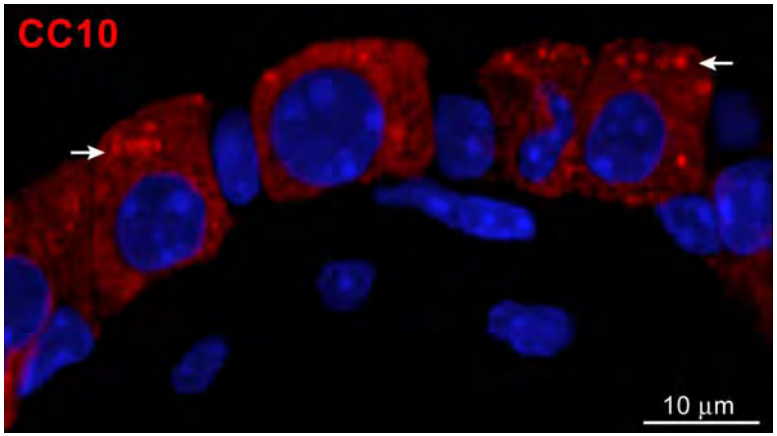

*CC10: This antibody was carefully selected because the antibody from Santa Cruz results in a nuclear localization of Clara cells which is not consistent with the secretory property of this protein. The specificity of the Abcam antibody is shown here in Clara cells at high magnification. Arrows point to secretory vesicles. Specificity was confirmed by spectral analysis.

Table 2. Magnitude of sampling and n Values

Parameter	n value	Aggregate sample size	Sample size (mean ± SD)
Adult human lung specimens			
Sample 1		98 mm^2	
Sample 2		124 mm^2	
Sample 3		75 mm^2	
Sample 4		112 mm^2	
Sample 5		84 mm^2	
Sample 6		55 mm^2	
Sample 7		66 mm^2	
Sample 8		104 mm^2	
Sample 9		126 mm^2	
Sample 10		226 mm^2	
Sample 11		238 mm^2	
Sample 12		174 mm^2	
All Samples	12	1,484 mm^2	124±57 mm^2
Bronchioles	12	508[a]	42±24[a]
c-kit positive hLSCs	12	454[b]	38±15[b]
Embryonic-fetal human lung specimens			
Sample 1		27 mm^2	

Sample 2		49 mm^2	
Sample 3		37 mm^2	
Sample 4		29 mm^2	
Sample 5		38 mm^2	
Sample 6		62 mm^2	
Sample 7		30 mm^2	
Sample 8		29 mm^2	
Sample 9		32 mm^2	
All Samples	9	332 mm^2	37±11 mm^2
c-kit positive hLSCs	9	230[b]	26±24[b]
hLSC Clones			
Limiting dilution	5	410[c]	82±14[c]
Single cell deposition	5	80[c]	16±8[c]
Immunophenotype of isolated hLSCs			
Immunocytochemistry			
Undifferentiated clonal hLSCs	4	16,774[d]	3,355±336[d]
Differentiated clonal hLSCs	4	6,415[d]	1,283±219[d]
FACS of hLSCs			
Hematopoietic markers	4	21,946[d]	5,487±510[d]
Mast cell markers	4	44,998[d]	11,250±2,030[d]
Mesenchymal cell markers	4	16,007[d]	4,002±465[d]
Undifferentiated non-clonal hLSCs	4	93,388[d]	23,347±4,986[d]
Undifferentiated clonal hLSCs	4	165,600[d]	41,400±6,551[d]

Differentiated clonal hLSCs	4	82,065[d]	20,516±2,530[d]
Pluripotency gene products	4	6,260[d]	1,565±289[d]
c-kit negative lung cells	4	12,433[d]	3,108±1,259[d]
bone marrow cells	3	19,376[d]	6,459±845[d]
hCSCs	4	16,078[d]	4,020±556[d]
Untreated injured lungs			
	4	6.3 mm^2	1.6±0.4 mm^2
Pulmonary repair			
Clonal hLSCs, 12 hours-2 days	4	396 mm^2	99±22 mm^2
Clonal hLSCs, 10-14 days	7	785 mm^2	112±31 mm^2
Non-clonal hLSCs, 10-14 days	14	1,221 mm^2	87±26 mm^2
HSCs, 10 days	6	129 mm^2	22±8 mm^2
hCSCs	6	114 mm^2	19±7 mm^2
c-kit negative human lung cells	6	109 mm^2	18±6 mm^2
Isolation of hLSCs from regenerated lung	17	N/A	N/A
Serial transplantation of clonal hLSCs	8	362 mm^2	46±13 mm^2
Two-photon microscopy			
Airway-perfused	5	8.1 mm^3	1.6±0.6 mm^3
Vasculature-perfused	5	9.8 mm^3	2.0±0.9 mm^3
Control mouse lung	3	4.6 mm^3	1.5±0.3 mm^3

[a] Number of bronchioles counted; [b] Number hLSCs identified; [c] Number of clones formed;

[d] Number of cells assessed; d, days; N/A, not applicable.